AGU100 ADVANCING EARTH AND SPACE SCIENCE

Tectonics

RESEARCH ARTICLE
10.1029/2017TC004808

Key Points:
- Punctuated rapid fault-related exhumation along inverted normal faults, separated by phases of slow cooling or subsidence
- ~110–90 Ma: exhumation of HP metamorphics along the northern branch of the Neo-Tethys; ~60–40 Ma: Kirşehir Block-Eurasia collision
- ~40–25 Ma: initial stages of the Arabia-Eurasia collision or trench advance; 4 ~11 Ma to present: onset of Anatolia westward motion

Supporting Information:
- Supporting Information S1

Correspondence to:
P. Ballato,
paolo.ballato@uniroma3.it

Citation:
Ballato, P., Parra, M., Schildgen, T. F., Dunkl, I., Yıldırım, C., Özsayın, E., et al. (2018). Multiple exhumation phases in the Central Pontides (N Turkey): New temporal constraints on major geodynamic changes associated with the closure of the Neo-Tethys Ocean. *Tectonics*, *37*, 1831–1857. https://doi.org/10.1029/2017TC004808

Received 12 SEP 2017
Accepted 7 MAY 2018
Accepted article online 21 MAY 2018
Published online 15 JUN 2018

Multiple Exhumation Phases in the Central Pontides (N Turkey): New Temporal Constraints on Major Geodynamic Changes Associated With the Closure of the Neo-Tethys Ocean

P. Ballato[1,2], M. Parra[3], T. F. Schildgen[1,4], I. Dunkl[5], C. Yıldırım[6], E. Özsayın[7], E. R. Sobel[1], H. Echtler[3], and M. R. Strecker[1]

[1]Institute of Earth and Environmental Sciences, University of Potsdam, Potsdam, Germany, [2]Now at Department of Science, University of Roma Tre, Rome, Italy, [3]Institute of Energy and Environment, University of Sao Paulo, Sao Paulo, Brazil, [4]Helmholtz-Centre Potsdam, GFZ German Research Centre for Geosciences, Potsdam, Germany, [5]Geoscience Center, University of Göttingen, Göttingen, Germany, [6]Eurasia Institute of Earth Sciences, Istanbul Technical University, Istanbul, Turkey, [7]Department of Geological Engineering, Hacettepe University, Ankara, Turkey

Abstract The Central Pontides of N Turkey represents a mobile orogenic belt of the southern Eurasian margin that experienced several phases of exhumation associated with the consumption of different branches of the Neo-Tethys Ocean and the amalgamation of continental domains. Our new low-temperature thermochronology data help to constrain the timing of these episodes, providing new insights into associated geodynamic processes. In particular, our data suggest that exhumation occurred at (1) ~110 to 90 Ma, most likely during tectonic accretion and exhumation of metamorphic rocks from the subduction zone; (2) from ~60 to 40 Ma, during the collision of the Kirşehir and Anatolide-Tauride microcontinental domains with the Eurasian margin; (3) from ~40 to 25 Ma, either during the early stages of the Arabia-Eurasia collision (*soft collision*) when the Arabian passive margin reached the trench, implying 70 to 530 km of subduction of the Arabian passive margin, or during a phase of trench advance predating *hard collision* at ~20 Ma; and (4) ~11 Ma to the present, during transpression associated with the westward motion of Anatolia. Our findings document the punctuated nature of fault-related exhumation, with episodes of fast cooling followed by periods of slow cooling or subsidence, the role of inverted normal faults in controlling the Paleogene exhumation pattern, and of the North Anatolian Fault in dictating the most recent pattern of exhumation.

1. Introduction

Mobile belts are long-lived deformation zones that develop along continental margins and hence represent first-order, lithospheric anisotropies that can favor strain localization under different tectonic regimes (e.g., Faccenna & Becker, 2010; Hyndman et al., 2005; McKenzie, 1972). Mobile belts may thus retain the fingerprints of multiple deformation events, providing unique insights not only into deformation styles and mechanisms but also mountain building processes and associated geodynamics. Such insights are particularly compelling in the realm of the Neo-Tethys Ocean, where different episodes of rifting, oceanic spreading, subduction, obduction, collision, oroclinal bending, and lateral extrusion of lithospheric blocks have occurred since the Late Mesozoic.

Located between the Arabia-Eurasia continental collision and the Hellenic subduction zones, the Turkish peninsula constitutes a mosaic of lithospheric blocks that have been progressively amalgamated since the Paleozoic, through the subduction of oceanic and continental lithosphere in association with multiple orogenic phases (Figure 1; e.g., Okay & Nikishin, 2015; Şengör & Yılmaz, 1981). Alternatively, Turkey can be considered a large Meso-Cenozoic accretionary orogen consisting of continental upper (and possibly lower) crust decoupled from subducted lower crustal and mantle lithospheric underpinnings (Pourteau et al., 2016; Van Hinsbergen et al., 2016). The Pontide mountains are one of the most prominent orogenic belts of Turkey, which were built over the former southern continental margin of the Eurasian Plate (Figure 1; for a recent review see Okay & Nikishin, 2015; Okay et al., 2017). This ~E-W oriented mountain range stretches along the northern coast of Turkey between the oceanic Black Sea Basin and the Tauride-Anatolide and the Kırşehir microcontinental domains (Figure 1; e.g., Okay et al., 2013; Pourteau et al., 2016; Van Hinsbergen et al., 2016) and exhibits a gradual westward decrease in mean elevation from over 3 km to few hundreds of meters

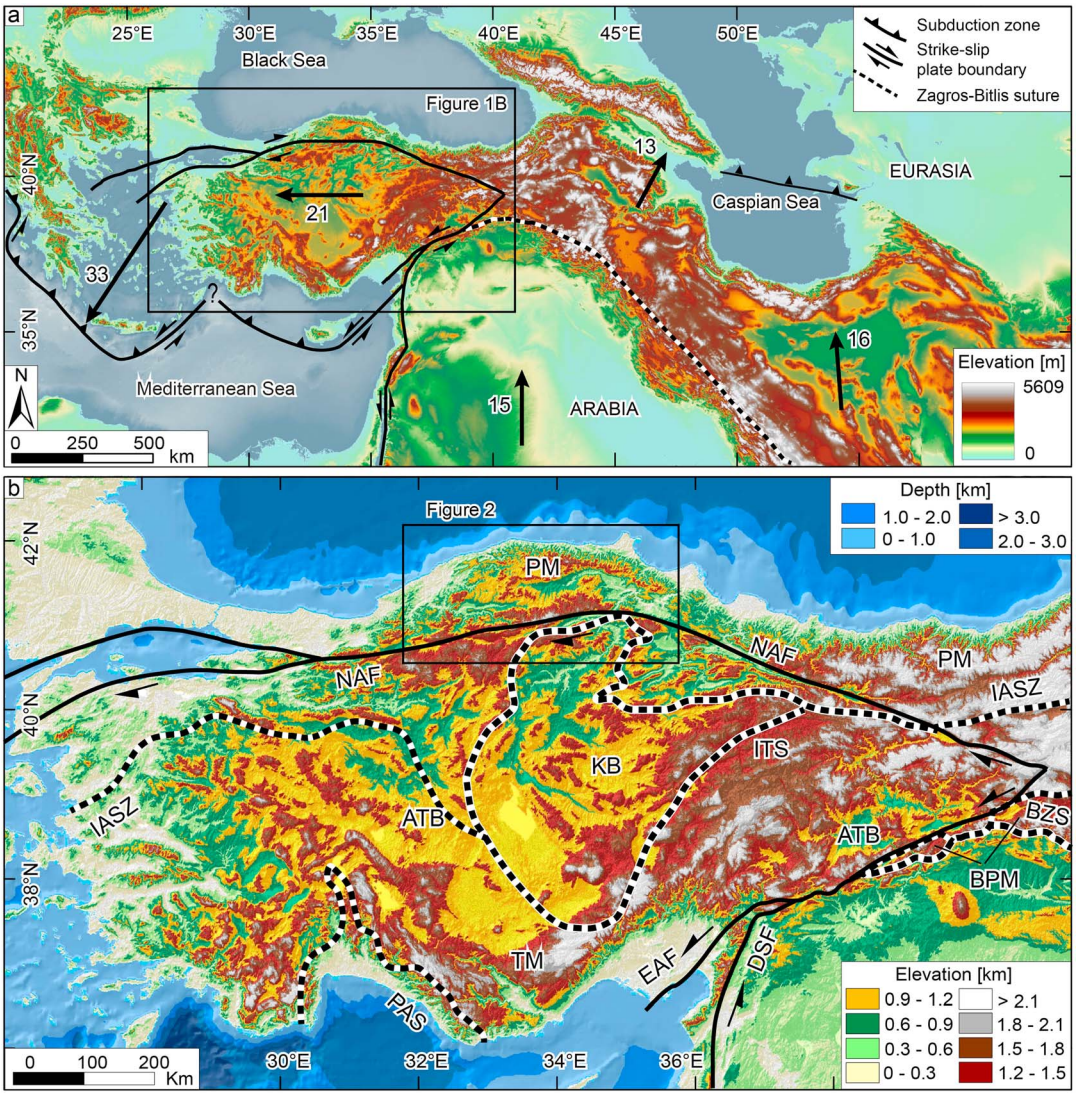

Figure 1. (a) Shuttle Radar Topographic Mission Digital Elevation Model (SRTM DEM) of middle east superimposed over a hillshade model. Black arrows and associated numbers indicate Global Positioning System-derived plate velocities (mm/year) assuming a fixed Eurasian plate (Reilinger et al., 2006). (b) DEM of Turkey including bathymetric data, showing the approximate location of major Tethyan sutures (Okay & Tüysüz, 1999). BSZ = Bitlis-Zagros Suture; IASZ = İzmir-Ankara-Erzincan Suture; ITS = Inner Tauride Suture; PAS = Pamphylia-Alanya Suture; DSF = Death Sea Fault; EAF = Eastern Anatolian Fault; NAF = North Anatolian Fault; ATB = Anatolian-Tauride Block; BPM = Bitlis-Pütürge continental Massif; KB = Kırşehir Block; PM = Pontide Mountains; TM = Tauride Mountains.

(Figures 1 and 2). The central sectors of the belt are composed of a suite of metamorphic, magmatic, and sedimentary rocks, documenting a complex geological history with episodes of subduction-related metamorphism, arc volcanism, and sedimentary basin development via normal faulting and lithospheric flexure throughout the Phanerozoic (Figure 3, e.g., Okay & Nikishin, 2015; Okay et al., 2017, and references therein). Although several studies have focused on this composite tectonostratigraphic, deformational, metamorphic, and magmatic history (e.g., Aygül et al., 2016; Çimen et al., 2017, 2018; Espurt et al., 2014; Frassi et al., 2018; Okay et al., 2006, 2013, 2014, 2015; Ustaömer & Robertson, 1997; Yıldırım et al., 2011), the timing of major Cenozoic events is only constrained by stratigraphic data. The spatially discontinuous nature of the sedimentary deposits, sedimentary hiatuses (Hippolyte et al., 2010, 2015; Okay et al., 2006, 2013, 2017; Tüysüz et al., 2012), and limited age information for continental sediments younger than the Late Eocene, however, does not allow us to reconstruct the most recent history of the Pontides and link it to the major geodynamic events. That history notably included the development of the North Anatolian Fault (NAF) and potential

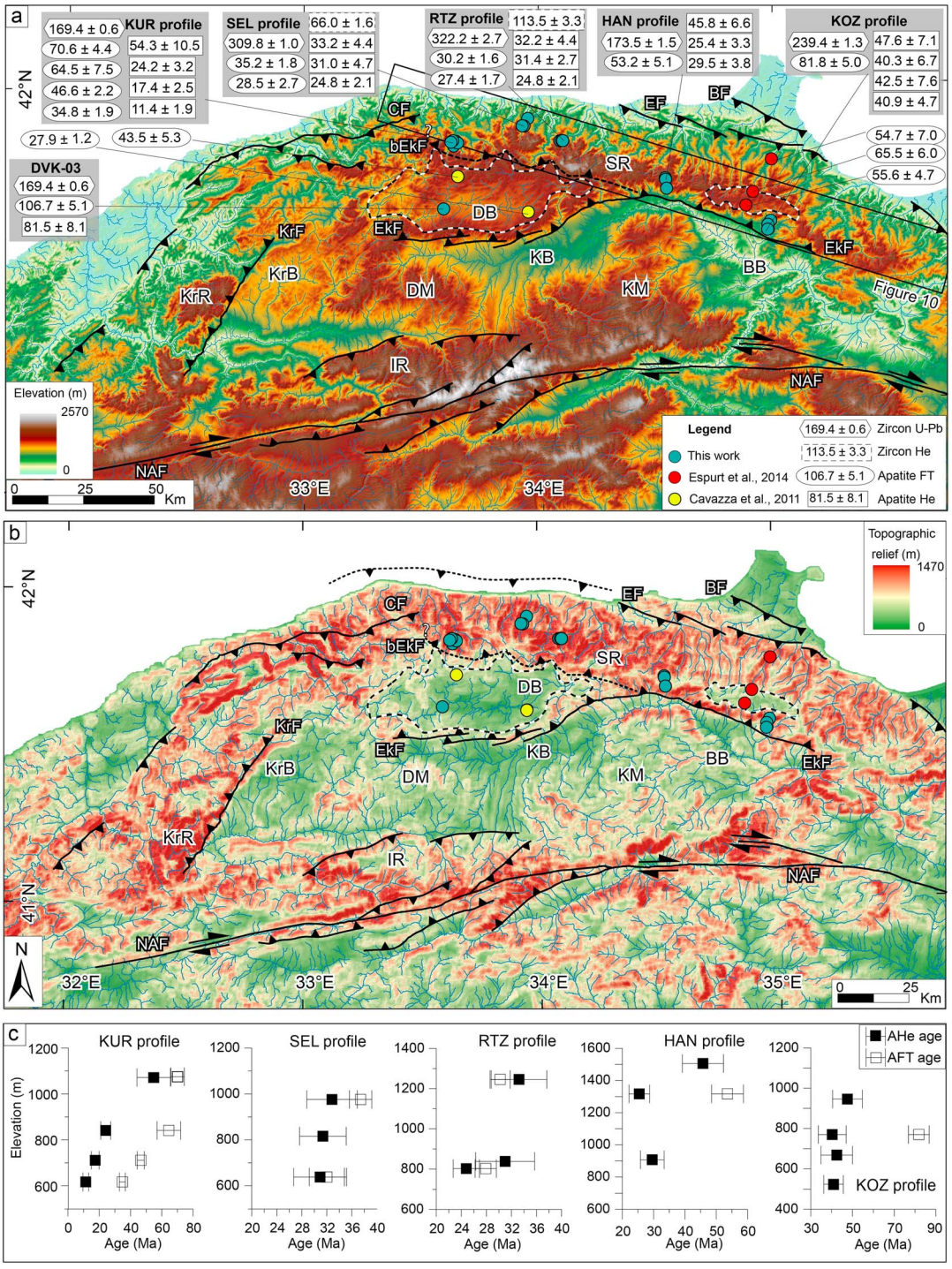

Figure 2. (a) Digital Elevation Model and (b) topographic relief map calculated over a 2-km circular radius superimposed over a hillshade model of the Central Pontides, showing major faults (modified after Yıldırım et al., 2011), Zircon U-Pb, AFT, and AHe ages. BF = Balıfakı Fault; CF = Cide Fault; EF = Erikli Fault; EkF = Ekinveren Fault; bEkF = Blind Ekinveren Fault; KF = Karabük Fault; NAF = North Anatolian Fault; IR = Ilgaz Range; KrR = Karabük Range; SR = Sinop Range; BB = Boyabat Basin; DB = Devrekani Basin; KrB = Karabük Basin; KB = Kastamonu Basin; DM = Daday Massif; KM = Kargı Massif. Note the arc-shaped, elevated, and high-relief topography of the Sinop and Karabük ranges (SR and KrR, respectively). These ranges are bounded by inward dipping reverse faults, extend parallel to the cost and tend to merge with the NAF and associated topography. Moreover, they delimit a semicircular and elevated low relief area that includes metamorphic massifs (DM and KM), Cretaceous to Eocene marine basins (BB, KrB, and DB) and a Mio-Pliocene continental basins (KB). (c) Age versus topographic elevation plots of vertical profile shown in Figure 2a. The dashed lines show the inferred location of a blind thrust fault defined in the text as the bEkF and the offshore continuation of the Erikli Fault.

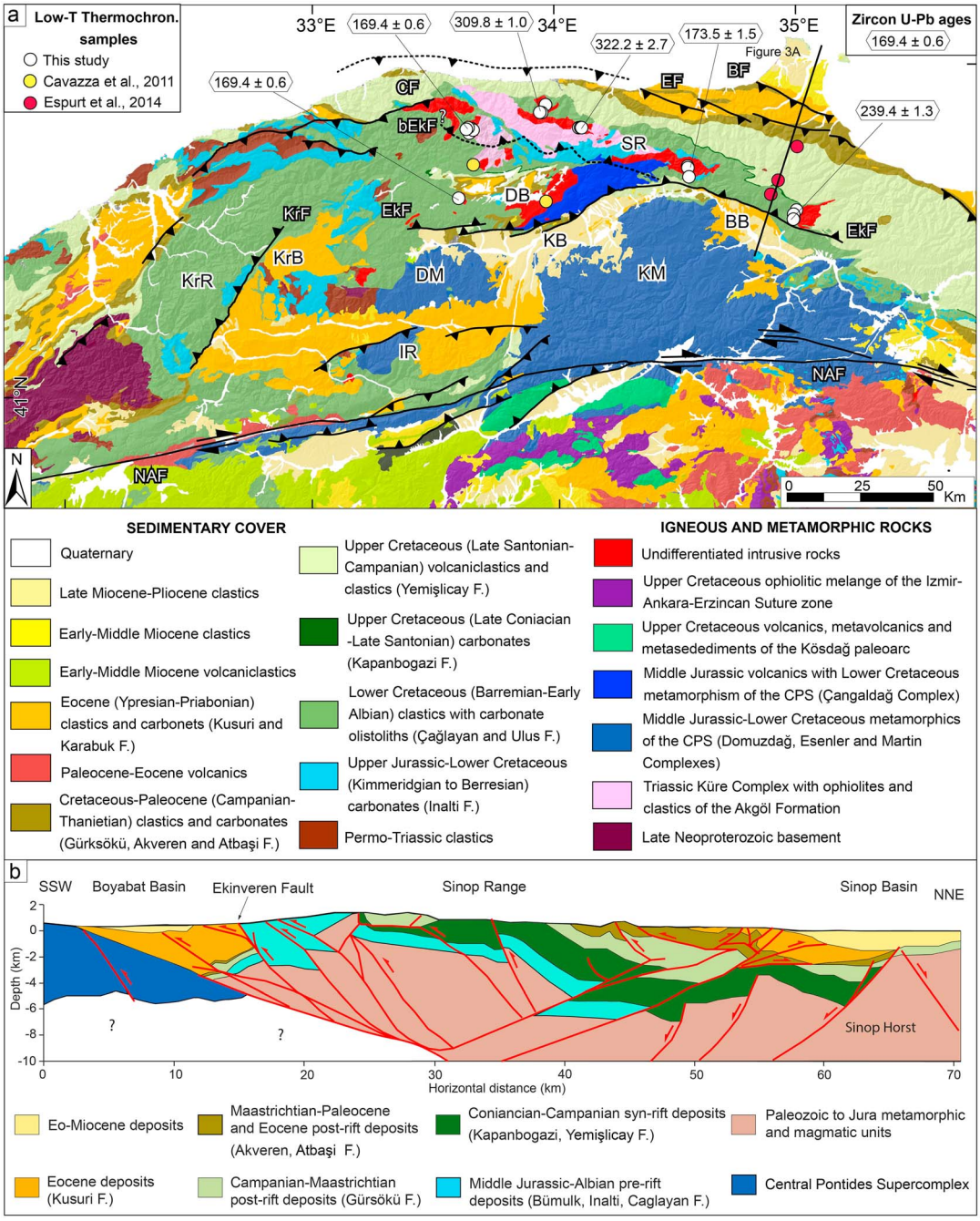

Figure 3. (a) Geologic map of Turkey redrawn after Şenel (2002), Okay et al. (2010), and Aygül and Oberhansli (2015). (b) Cross section of the Central Pontides based on seismic lines (redrawn after Espurt et al., 2014). Note that the Sinop Horst marks the transition between tectonically inverted and not inverted areas.

topographic growth of the Central Pontides associated with transpression (Ellero et al., 2015; Schildgen et al., 2014; Yıldırım et al., 2011; Yıldırım, Melnick, et al., 2013; Yıldırım, Schildgen, et al., 2013).

To unravel the geological history of the Central Pontides in the framework of collisional tectonic and plateau building processes, we have performed a geochronology and low-temperature thermochronology study including zircon U-Pb, apatite fission track (AFT), zircon and apatite (U-Th-Sm)/He (AHe) dating of granitoides exposed along five vertical profiles spanning up to 600 m of topographic relief. Overall, our new data document the spatiotemporal pattern of fault-related exhumation during major Late Mesozoic to Cenozoic

deformation events and the role of inherited structures in controlling those events. Furthermore, our data provide new insights into the geodynamic processes that triggered fault-related exhumation.

2. Tectonostratigraphic Evolution of the Central Pontides

The Central Pontide mountains are characterized by a suite of metamorphic, magmatic, sedimentary, and mantle rocks, which recorded a prolonged and complex Late Paleozoic to Early Cenozoic history of subduction, microcontinent collision, and backarc extension (Figure 3; e.g., Aygül & Oberhansli, 2015; Aygül et al., 2016; Çimen et al., 2018, 2017; Okay et al., 2017, 2013, 2006; Okay & Nikishin, 2015). The Late Paleozoic episodes include the northward subduction of the Paleo-Tethys oceanic lithosphere beneath southern Laurasia, in association with arc magmatism at ~350 to 300 Ma and the Carboniferous to Permian collision with Armorica type terrains (Variscan orogeny) that led to the development of Pangea (e.g., Okay & Nikishin, 2015; Stampfli & Borel, 2002, and references therein). These events were followed by Late Permian to Early Triassic rifting and volcanism that caused opening of the Neo-Tethys Ocean and the establishment of new subduction zone (s), with the ultimate amalgamation of the Cimmerian blocks to the southern Eurasian margin (Cimmerian orogeny; e.g., Şengör, 1991; Şengör & Yılmaz, 1981; Stampfli & Borel, 2002; Zanchi et al., 2009). In the Central Pontides, this amalgamation is thought to have caused the Late Triassic accretion of an oceanic plateau without the involvement of continental lithosphere (e.g., Okay et al., 2006; Okay & Nikishin, 2015; Ustaömer & Robertson, 1994, 1997). The oldest rocks recording this orogenic episode are Upper Triassic to possibly Lower Jurassic distal trench turbidites of the Akgöl Formation (~210 to 199 Ma), which were deposited onto basaltic pillow lavas (Okay et al., 2006, 2015). These synorogenic deposits are exposed in the Sinop range and form the Küre Complex (Figure 3; Ustaömer & Robertson, 1994), which was intruded by Middle-Upper Jurassic (post Cymmerian) granitoids (~174 to 158 Ma; e.g., Okay et al., 2006, 2013, 2014, 2015, 2017).

From the Late Jurassic to the Early Cretaceous, a marine transgression occurred, leading to the deposition of the shallow-water marine limestones of the İnaltı Formation (Kimmeridgian to Berresian, ~155 to 140 Ma, up to 1 km of thickness; Derman & İztan, 1997), a regional stratigraphic marker that can be followed from Crimea to Iran (e.g., Okay & Nikishin, 2015). After the deposition of the İnaltı Formation, a Middle Jurassic oceanic volcanic complex (Çangaldağ Complex; Çimen et al., 2018, 2017; Okay et al., 2014; Ustaömer & Robertson, 1997), which experienced Early Cretaceous (Valanginian to Barremian, ~135 to 122 Ma) low-greenschist facies metamorphism, was accreted to the southern margin of the Eurasian plate during northward directed subduction (Figure 3; e.g., Okay et al., 2006, 2013). Over a similar time interval (Barremian to earliest Albian, ~130 to 110 Ma), a sequence of turbidites reflecting a submarine fan system at least 3-km thick (Çağlayan Formation) was deposited over a wide region of the modern Central Pontides. These sedimentary deposits contain kilometers-scale olistoliths (mostly from the İnaltı Formation) sourced from the north and therefore have been interpreted to represent deposition in a forearc and trench setting, most likely during a nonmagmatic rifting episode that predated the opening of the back-arc Black Sea Basin (e.g., Derman & İztan, 1997; Görür & Tüysüz, 1997; Hippolyte et al., 2010, 2015; Okay et al., 2006, 2013; Tüysüz et al., 2012). Subsequently, an Albian to Coniacian (~113 to 90 Ma) phase of tilting caused erosion of the Çağlayan Formation turbidites. This episode has been linked to tectonic accretion and exhumation of an imbricated, south verging system of metamorphosed (high pressure and low temperature) oceanic and mantle rocks (Domuzdağ Complex) and Lower Cretaceous metasediments (blueschist and greenschist of the Esenler and the Martin complexes) between 110 and 92 Ma (Central Pontides Supercomplex, Figure 3; Aygül et al., 2016; Okay et al., 2006, 2013). Farther south, the occurrence of ~95 Ma volcanic and sedimentary rocks that recorded low-grade metamorphism at ~70 Ma suggests the development of a magmatic arc, most likely associated with a northward dipping, intraoceanic subduction zone between the Central Pontides Supercomplex and Gondwana-derived blocks of Central Anatolia (Figure 3; Kösdağ paleoarc, Aygül & Oberhansli, 2015; see also Gürer et al., 2016; Van Hinsbergen et al., 2016).

At the same time, backarc extension and rifting led to the fragmentation of the former southern Eurasian margin with the opening of the Black Sea (Espurt et al., 2014; Görür & Tüysüz, 1997; Nikishin et al., 2003; Nikishin, Okay, Tüysüz, Demirer, Amelin, & Petrov, 2015; Nikishin, Okay, Tüysüz, Demirer, Wannier, et al., 2015; Okay et al., 1994, 2013; Tüysüz et al., 2012; Zonenshain & Le Pichon, 1986). This event is well documented by the deposition in unconformity of an up to 160-m-thick package of Late Coniacian to Santonian reddish pelagic mudstone (Kapanboğazı Formation; ~88 to 84 Ma) and an up to 2-km-thick sequence of latest Santonian to earliest Campanian volcaniclastic turbidites (Yemişliçay Formation; ~84 to 82 Ma; Figure 3;

Derman & İztan, 1997; Hippolyte et al., 2015; Leren et al., 2007; Okay et al., 2006, 2013), sourced from submarine volcanos located north of the modern shoreline (Nikishin, Okay, Tüysüz, Demirer, Amelin, & Petrov, 2015; Nikishin, Okay, Tüysüz, Demirer, Wannier, et al., 2015). Along the northern flank of the Sinop Range, volcaniclastic sedimentation was followed by the deposition of an up to 5-km-thick sequence of calcareous and siliciclastic deep-water turbidites passing southward to shallow-water marine limestone that postdates oceanic spreading in the Black Sea (Gürksökü, Akveren, Atbaşı, and Kusuri formations; Campanian to the Middle Eocene; ~83 to 40 Ma; Figure 3; Derman & İztan, 1997; Görür & Tüysüz, 1997; Hippolyte et al., 2010, 2015; Janbu et al., 2007; Leren et al., 2007; Nikishin, Okay, Tüysüz, Demirer, Amelin, & Petrov, 2015; Nikishin, Okay, Tüysüz, Demirer, Wannier, et al., 2015; Okay et al., 2013; Özcan et al., 2012). Along the southern flank of the Sinop Range, these sediments are thinner (possibly up to 1- to 2-km thick) and contain angular unconformities and disconformities that testify to episodic contractional deformation throughout the Late Cretaceous to Early Cenozoic (Hippolyte et al., 2015; Okay et al., 2006, 2013).

Thick ($>$ 4 km) Upper Cretaceous to Eocene marine sediments are currently exposed in the hanging wall of the north dipping Ekinveren and Karabük thrust faults (Figure 3). To the south, in their footwalls, a discontinuous and thinner sequence including Upper Cretaceous, Paleocene, and Lower to Middle Eocene (Ypresian to Priabonian; ~53–50 to 40 Ma) shallow-water marine clastics and limestones unconformably cover rocks of the Central Pontides Supercomplex (Figure 3; Görür & Tüysüz, 1997; Hippolyte et al., 2010; Okay et al., 2013; Özgen-Erdem et al., 2005; Özcan et al., 2007). This relationship suggests that the interior of the modern Central Pontides must have been dominated by periods of erosion or nondeposition, at least until ~53–50 Ma, when shallow-water marine conditions were established (Figure 3). Renewed subsidence has been interpreted to reflect the development of piggyback basins (Hippolyte et al., 2010) during the inversion of the Black Sea passive margin, which was triggered by the collision between the Kırşehir Block and the Eurasian Plate (e.g., Cavazza et al., 2011; Espurt et al., 2014; Kaymakçı et al., 2009; Okay et al., 2013; Özcan et al., 2007; Özgen-Erdem et al., 2005; Van Hinsbergen et al., 2016). Furthermore, paleomagnetic data suggest that oroclinal bending processes, which have been interpreted to reflect collision and indentation of the Kırşehir Block, occurred between the latest Cretaceous and the earliest Paleocene (Meijers et al., 2010). After the deposition of the ~53–50 to 40 Ma shallow-water marine clastics and limestones, the region experienced widespread erosion at least until the development of the Kastamonu intermontane basin (Yıldırım et al., 2011; Yıldırım, Melnick, et al., 2013). This erosion has been linked to transpressional motion along the northward convex sector of the North Anatolian Fault (NAF; Figure 1), which should have also promoted renewed rock uplift, localized river incision, and overall topographic growth of the Central Pontides (Figures 2 and 3; Ellero et al., 2015; Schildgen et al., 2014; Şengör et al., 2005; Yıldırım et al., 2011; Yıldırım, Melnick, et al., 2013; Yıldırım, Schildgen, et al., 2013). This renewed activity has been suggested to have occurred during the last ~5 Ma (although the timing is weakly constrained) through the development of a north verging orogenic wedge connected through a shallow dipping detachment to the NAF (Yıldırım et al., 2011).

3. Topography, Structural Setting, and Active Tectonics

The topography of the Central Pontide mountains rises from the Black Sea coast to ~1.5 to 1.8 km of elevation over 25 to 50 km (Sinop and Karabük ranges, Figure 2) and constitutes a prominent orographic barrier to moist air masses sourced from the Black Sea (Figures 1 and 2; Schemmel et al., 2013), which formed sometime during the last 8 Ma (Mazzini et al., 2013). The arc-shaped range accommodates up to 6 mm/year of shortening with a strong E-W gradient between 31 and 35°E longitude (Reilinger et al., 2006; Yıldırım et al., 2011), which is accommodated along inward dipping thrusts.

Within the Central Pontides, along the E-W to WNW-ESE oriented Sinop Range, the northward dipping Ekinveren Thrust appears to have accommodated a significant fraction of Cenozoic shortening and uplift, which in turn has led to the erosion of the Upper Cretaceous-Lower Eocene sequence and the exposure of the Çangaldağ and Küre complexes (Figure 3). Moreover, the Ekinveren Thrust is associated with a system of north dipping splay faults on both its hanging wall and footwall, especially in proximity to the Boyabat and Kastamonu basins (Figures 2 and 3; Espurt et al., 2014; Görür & Tüysüz, 1997; Okay et al., 2006; Yıldırım et al., 2011). Conversely, the system of southward dipping faults exposed near the shoreline (Erikli and Balıfakı faults and their possible westward offshore continuation) have accommodated a minor amount of

dip-slip motion and hence appear to constitute second-order structures (Figures 2 and 3). In the NE-SW oriented Karabük Range (Ulus Basin; e.g., Hippolyte et al., 2010), motion along the NW dipping Karabük Fault has led to the erosion of the Upper Cretaceous-Lower Eocene synrift to postrift sedimentary sequence and the exposure of Upper Jurassic-Lower Cretaceous sediments (Figure 3). Toward the shoreline, a system of southward-, shallow-dipping thrusts has led to folding and exhumation of Permian clastic sediments (Figures 2 and 3; e.g., Cide Fault). Deformation continues offshore along the Central Pontides through a system of southward-dipping thrust faults, as suggested by uplifted marine terraces (Yıldırım, Melnick, et al., 2013), instrumental seismicity (the 1968 Bartın earthquake, Alptekin et al., 1986) and seismic reflection lines (Yıldırım et al., 2011, and references therein). It should be noted, however, that this submarine fold and thrust belt appears to have accommodated limited shortening (e.g., Nikishin, Okay, Tüysüz, Demirer, Amelin, & Petrov, 2015; Nikishin, Okay, Tüysüz, Demirer, Wannier, et al., 2015; Rangin et al., 2002) and hence cannot be associated with significant underthrusting of the Black Sea Basin beneath the Pontides. Furthermore, these contractional structures seem to be rather localized, because east and north of the Sinop Basin (Figure 3), normal faults cut supposed Early Cenozoic contractional structures (Özhan, 1989; Rangin et al., 2002).

The eastern sector of the Sinop Range and parts of the Karabük Range (hanging wall of the Ekinveren and Karabük thrust faults, respectively) are capped by low-relief ($<$300 m) erosional remnants that have been uplifted to elevations $>$1,000 m and locally tilted (Figure 2; Yıldırım et al., 2011). These patches, which are thought to represent the vestige of a regional, low-elevation paleosurface that experienced differential uplift (Yılmaz, 2007), are also found to the south of these ranges, in the footwall of the Ekinveren and Karabük thrust faults at elevations of 600 to 1,000 m (Figure 2). In the Devrekani Basin (hanging wall of the Ekinveren Thrust), these erosional remnants cut Middle-Late Eocene shallow-water marine sediments (Figures 2 and 3), implying that they must have formed after ~40 Ma.

Farther south, the E-W to WNW-ESE and the NE-SW oriented Sinop and Karabük ranges merge into an E-W oriented system of high ridges (including the $>$2-km-high Ilgaz Range), which are bounded to the south by the NAF. These mountain ranges arose from transpressional deformation across the restraining bend of the NAF and exhibit northward-directed thrusting (Ellero et al., 2015; Yıldırım et al., 2011).

4. Methodology

To unravel the Cenozoic spatiotemporal pattern of fault-related exhumation, we have combined low-temperature thermochronology, including apatite fission track (AFT), zircon and apatite (U-Th-Sm)/He (ZHe and AHe, respectively), and geochronology (zircon U-Pb) with thermal modeling using HeFTy (Ketcham, 2005; Ketcham et al., 2017). Thirty-six samples were collected from five elevation profiles spanning 400 to 800 m of topographic relief along the Sinop Range (Sakarya Zone; Figures 2 and 3). Most of the sampled granitoids were mapped as Jurassic or Cretaceous (Şenel, 2002), but according to recent isotopic ages (Okay & Nikishin, 2015, and references therein), the rocks we sampled have Carboniferous (RTZ and SEL samples) and Middle-Late Jurassic emplacement ages (Küre Complex, KUR samples; Çangaldağ Complex, HAN samples; Devrakani Basin, DVK samples). Rocks from the easternmost profile (KOZ samples) have not been dated, but available geological maps assign them a Late Cretaceous age (Şenel, 2002). Mineral separation was performed at the University of Potsdam following standard protocols including crushing, sieving, water table, magnetic, and heavy-liquid separation. Although most of the samples were relatively rich in zircons, only 50% of the samples yielded enough apatite grains for analysis.

4.1. Zircon U-Pb Analysis

Six samples (one from each elevation profile and one from the Devrekani Basin) were selected for zircon U-Pb dating with laser-ablation inductively coupled plasma mass spectrometry (LA-ICP-MS), which was carried out at the Institute of Geosciences of the University of São Paulo (Brazil). Zircon grains were mounted into epoxy resin discs and surveyed for internal compositional zonations and/or inclusions via cathodoluminescence and transmitted light imaging. Fifteen to thirty-five zircon grains were measured for each sample according to their abundance and age reproducibility. The U-Pb isotope analyses were performed using a ThermoFisher Neptune LA-ICP-MS equipped with a 193 Photon laser system (Sato et al., 2010). The analytical routine included three measurements of GJ standard, two blanks, and two NIST 612 standards, followed by 13 analyses of zircons with unknown age, and two additional analysis of GJ standard, two blanks, and two NIST

Table 1
Summary of Zircon U-Pb, AFT, and AHe Ages

Sample code	ZHe (Ma)	Error (Ma)	# Gr	AFT (Ma)[a]	Error (Ma)	# Gr	P (c2) (%)[b]	Length (mm)	1 s (mm)	# length	AHe (Ma)	Error (Ma)	# Gr	UPb (Ma)	Error (Ma)	MSWD	# Gr	Elev. (m)	Lat. (°)	Long. (°)	Lithology
DVK-03				106.7	5.1	20	82.7	15.51	0.83	13	81.5	8.1	3	169.4	0.6	0.44	13	982	41.623267	33.59230	Granodiorite
KUR-01				70.6	4.4	27	5.6	10.21	3.88	3	54.3	10.5	2					1075	41.82370	33.63670	Granodiorite
KUR-11				64.5	7.5	18	19.5	13.70	3.12	14	24.2	3.2	3	169.4	0.6	0.02	26	841	41.83753	33.64623	Granodiorite
KUR-04				46.6	2.2	25	0.0	13.76	1.12	47	17.4	2.5	2					711	41.83305	33.65270	Granodiorite
KUR-08				34.8	1.9	21	53.8	11.6	NA	1	11.4	1.9	3					617	41.84002	33.63283	Granite
RTZ-03				30.2	1.6	20	7.3	13.3	2.15	100	33.2	4.4	3	322.2	2.7	1.3	20	1246	41.83668	34.08795	Granodiorite
RTZ-02											31.0	4.7	2					838	41.83738	34.09600	Granodiorite
RTZ-01	113.5	3.3	4	27.4	1.7	20	12.1	13.02	2.10	84	24.8	2.1	2					802	41.83675	34.10001	Granodiorite
SEL-05				35.2	1.8	19	10.4	13.79	1.47	100	32.8	4.0	3	309.8	1.0	0.35	20	976	41.90932	33.95225	Granite
SEL-06											31.4	3.7	2					816	41.88472	33.93627	Granite
SEL-02	66.0	1.6	3	28.5	2.7	19	9.5	12.84	2.63	8	30.9	4.2	2					638	41.88570	33.92810	Pegmatite
HAN-01											45.8	6.6	3					1506	41.70820	34.53480	Granodiorite
HAN-03				53.6	5.1	25	71.5	12.61	2.44	21	25.4	3.3	3	173.5	1.5	0.02	12	1317	41.71303	34.53381	Granodiorite
HAN-07											29.5	3.8	3					907	41.68003	34.53838	Granodiorite
KOZ-04											47.6	7.1	3	239.4	1.3	0.54	7	946	41.57098	34.97650	Granodiorite
KOZ-01				81.8	5	23	28.6	13.55	2.02	99	40.3	6.7	3					770	41.54515	34.96435	Granodiorite
KOZ-03											42.5	7.6	3					668	41.55870	34.96416	Granodiorite
KOZ-02											40.9	4.7	3					523	41.54308	34.96288	Granodiorite

Note. Errors for AHe data are presented as standard error for samples with three aliquots and as standard deviation for samples with two aliquots.
[a]Pooled (central) age reported for ages that pass (fail) the c2 test (<5%). [b]Pc2 (%) is the chi-square probability (Galbraith, 1981; Green, 1981). Values greater than 5% are considered to pass it and represent a single population of ages.

standards. The raw data were then corrected for background, instrumental mass bias drift and common Pb using an in-house spreadsheet OR software (Siqueira et al., 2014). Results are shown in Table 1, and the data are portrayed in concordia and PDP diagrams generated with Isoplot/Ex (Ludwig, 2003; supporting information Figures S1 to S6). The complete data set is reported in the supporting information Tables S1 to S6).

4.2. Apatite Fission Track Analysis

Eleven samples were selected for AFT analysis, with approximately 20 grains per sample analyzed using the external detector method (Gleadow & Duddy, 1981). Nine samples were dated with the Autoscan system (Gleadow et al., 2009), using manual counting, at the Federal University of Rio Grande do Sur (Brazil) and two samples using the FTStage system (Dumitru, 1993) at the University of São Paulo (Brazil). Data are reported as pooled ages with ±1σ except when they failed the chi-square test (P (χ^2) ≥ 5%; Galbraith, 1981), in which case the central age is reported. Fission track length measurements were facilitated by heavy-ion irradiations in seven samples, as described in Jonckheere et al. (2007). The size of the etch-pit diameter parallel to the c axis (Dpar) was measured and used as a kinetic parameter for the thermal history modeling (Donelick et al., 1999; Ketcham et al., 1999). Results are shown in Table 1, and the analytical details are provided in the supporting information (SI7).

4.3. Apatite and Zircon (U-Th-Sm)/He Analysis

Nineteen apatite and two zircon samples, consisting of at least three single-crystal aliquots each, were analyzed at the GÖochron Laboratories of the University of Göttingen. After careful inspection under a microscope at 250X magnification and with cross-polarized light, euhedral grains that exceeded 70 μm in width were selected. The shape parameters were determined and archived by multiple digital microphotographs. Crystals were wrapped in platinum capsules and heated in the full-metal extraction line by an infrared laser under high vacuum. The extracted gas was purified using a SAES Ti-Zr getter kept at 450 °C. The chemically inert noble gases and a minor amount of other gases were then expanded into a Hiden triple-filter quadrupol mass spectrometer equipped with a positive ion counting detector. Crystals were additionally checked for degassing of He by sequential reheating and He measurement. Following degassing, samples were retrieved from the gas extraction line, spiked with calibrated ^{230}Th and ^{233}U solutions and dissolved. Spiked solutions were analyzed by isotope dilution on a Perkin Elmer Elan DRC II ICP-MS with an APEX microflow nebulizer. The ejection correction factors (F_t) were determined for the single crystals by a modified algorithm of Farley et al. (1996) using an in-house spreadsheet. The (U-Th-Sm)/He ages were calculated by the Taylor Expansion Method (Braun et al., 2006). The Sm content was also considered for age calculation. Results are presented in Table 1, while the complete data set is shown in the supporting information (S8 and S9).

4.4. Thermal-History Modeling

Inverse thermal modeling programs (e.g., HeFTy, Ketcham, 2005;s Ketcham et al., 2007, 2009; and QTQt, Gallagher, 2012) offer the possibility to investigate time-temperature paths that are consistent with thermochronology data and hence evaluate potential exhumation histories. In the newest version of HeFTy (v. 1.9.1, Ketcham et al., 2017), it is possible to perform thermal modeling of not only single samples but also elevation profiles of samples,

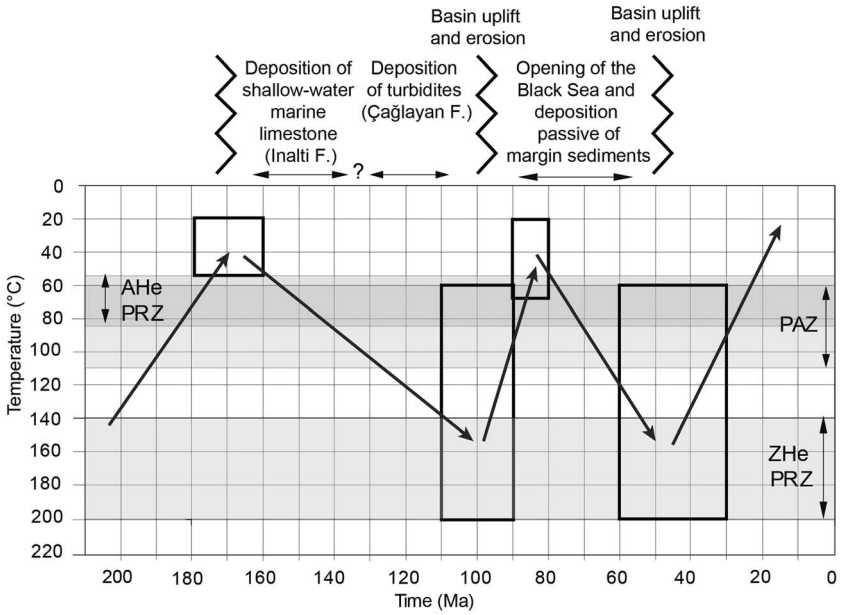

Figure 4. Time-temperature diagram showing the constraint boxes used in the thermal modeling according to major depositional and erosional events (see section 4.4 for details).

considering the most elevated sample to be at 0-m elevation (equivalent to the top of a well) and the lower samples as down-well samples. Although thermal histories from inverse models do not directly consider perturbations of the geothermal gradient associated with topographic changes, variations in erosional efficiency, or shear heating and advection during faulting (e.g., Ehlers & Farley, 2003; Willett & Brandon, 2013), they appear to provide robust and consistent thermal histories (Ketcham et al., 2017).

To constrain the Cenozoic cooling history of the Central Pontides, we performed single and multisample thermal modeling with HeFTy by integrating available stratigraphic information, paleothermometric data, and additional geological constraints with our new geochronology and low-temperature thermochronology data. Our input parameters included AFT (single grain ages, projected track lengths, and Dpar values), ZHe, and AHe data (mean age of at least two aliquots with 2σ error). We assumed a mean surface temperature of 10 ± 5 °C, and for the multisample modeling, the present-day temperature of each sample was calculated according to their relative down-well position (see above) assuming a geothermal gradient of 25 °C/km (Starostenko et al., 2014). The segments between the constraint boxes were set to be monotonic consistent, (gradual/episodic during heating/cooling) and in few cases monotonic variable (but only during cooling). The AFT annealing model for AFT data is from Ketcham et al. (2007), whereas the diffusion model for AHe data is from Farley (2000). Finally, the halving between paths was set to two or three depending on the supposed complexity of the thermal history inferred by stratigraphic data. Each model was run until 100 *good paths* (i.e., paths with goodness of fitness, GOF, greater than 0.5 were found). For some multisample modeling, however, it was not possible to obtain 100 good paths and hence models where stopped after 100 *acceptable paths* (i.e., paths with GOF between 0.15 and 0.5).

For the oldest part of the thermal histories, we considered the simplest possible scenario with monotonic cooling starting from our U-Pb ages at ~500 °C to temperatures of 20–60 °C (shallow depths) during the Late Jurassic to Early Cretaceous. This time-temperature window corresponds to the deposition of the shallow-water marine limestones of the İnaltı Formation (~155–135 Ma) over a heterogeneous substratum comprising our analyzed granitoids (Figure 4). The pre-Late Jurassic time-temperature paths are not discussed in the text because a detailed characterization of the oldest thermal history of our samples is beyond the scope of this study, and the multisample thermal modeling does not allow modeling thermal histories from temperatures of zircon crystallization (>750 °C; Harrison et al., 2007). The subsequent constraint box was placed between 110 and 90 Ma when a first phase of basin uplift and erosion occurred after the

10.1029/2017TC004808

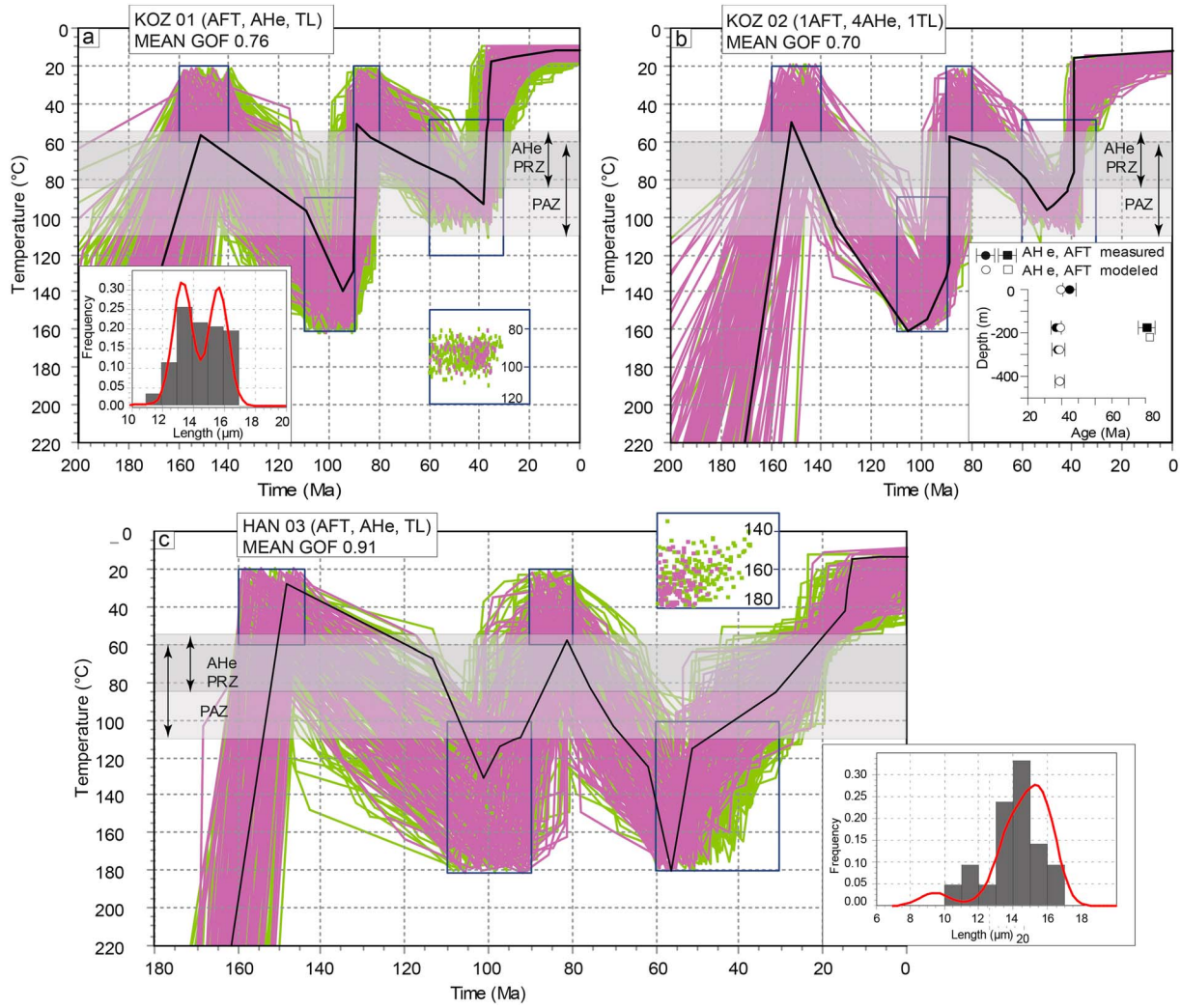

Figure 5. Inverse thermal modeling results for sample KOZ-01 (a), the KOZ vertical profile (b, lowermost sample of the profile) and sample HAN-03 (c) with acceptable (green) and good (magenta, 100 paths) time-temperature paths and the best fit model (black line). The data set used for each modeling and the mean GOF is indicated in the plot heading (with TL indicating track lengths). The insets of Figures 5a and 5c show constraint points (i.e., points marking the onset of cooling) for the 60- to 30-Ma constrain box, measured (gray histograms) and modeled (red line) track length distributions. For the multisample modeling (b), the inset represents the vertical profile considering a down-well setting (i.e., with the topmost sample at 0 m of elevation), with modeled and measured ages. Each model started from our U-Pb ages (Table 1) at ~500 °C.

deposition of the Çağlayan Formation (Figure 4; e.g., Hippolyte et al., 2010, 2015; Okay et al., 2013, 2017). This constraint box was imposed on all models including those (HAN, KOZ, and SEL samples) where our deepest thermochronometer was reset during the Late Cretaceous-Paleocene burial (Figure 4). The next constraint box was placed between 90 and 80 Ma, when rifting associated with the opening of the Black Sea started (Kapanboğazı Formation; Figure 4). Finally, a constraint box marking the onset of basin inversion was imposed between 60 and 30 Ma (Figure 4; Espurt et al., 2014; Hippolyte et al., 2010, 2015; Okay et al., 2013, 2017). The modeling was then implemented according to vitrinite reflectance and organic geochemistry (e.g., rock-eval pyrolysis, total organic carbon, and n-alkane distribution) data from the Lower Cretaceous turbidites of the Çağlayan Formation (Derman & İztan, 1997; Görür & Tüysüz, 1997; Korkmaz et al., 2013). Although sparse, these data document an overall westward increase of peak temperatures at the base of the Çağlayan Formation from ~100 °C in the eastern sectors of the study area (HAN and KOZ samples; Figure 5) to temperatures of ~160 °C in central sectors (RTZ and SEL samples; Figure 6).

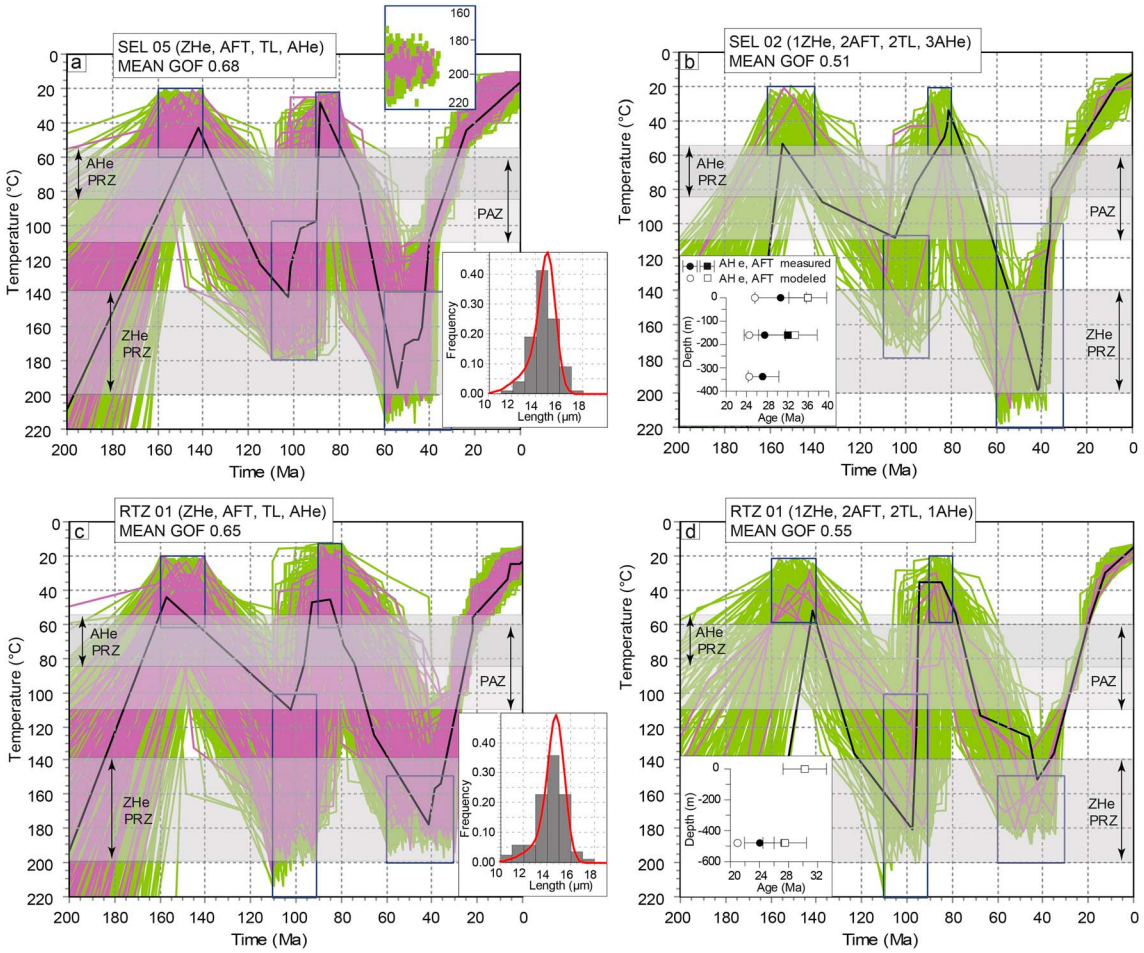

Figure 6. Inverse thermal modeling results for samples SEL (a = single sample and b = multisample modeling) and RTZ (c = single sample and d = multisample modeling; see caption of Figure 5 for details). Note that multisample modeling of SEL and RTZ vertical profile modeling was interrupted after 100 acceptable paths because it was not possible to find 100 good paths despite the large number of tried paths.

5. Results

5.1. Geochronology and Low-Temperature Thermochronology Data

5.1.1. KOZ Profile

The easternmost profile includes four granodiorite samples spanning ~400 m of relief (KOZ samples; Figures 2 and 3). This intrusive body has been dated for the first time in this study through zircon U-Pb analysis and has yielded multiple ages (KOZ04). A few zircon crystals appear to be older than 300 Ma, while one population of five grains has a concordant U-Pb age of 298.2 ± 1.9 Ma (MSWD = 0.21), most likely reflecting recycling of Late Carboniferous zircons associated with the Variscan orogenesis. The youngest population (seven grains) has a concordant U-Pb age of 239.4 ± 1.3 Ma (MSWD = 0.54), which correlates with the Triassic arc magmatism that occurred regionally during the Cimmerian orogenesis (Okay & Nikishin, 2015). Interestingly, although Triassic zircons are the dominant clastic population in coeval turbidites (e.g., Okay & Nikishin, 2015), our sampled granitoid appears to be the first documented Triassic intrusive body of the Black Sea region. Along the same transect, one sample was analyzed with AFT and four with AHe. The AFT cooling age is 81.8 ± 1.5 Ma, with a mean track length of 13.55 ± 2.02 μm based on 99 measurements. The four AHe ages exhibit relatively good reproducibility, with cooling ages ranging from 47.6 ± 7.1 to 40.3 ± 6.7 Ma.

5.1.2. HAN Profile

Located ~50 km west of the KOZ profile and with an elevation range of ~600 m, the HAN profile (Çangaldağ Complex; Figures 2 and 3) yielded a U-Pb zircon population of 12 grains (out of 26 analyzed) with a

concordant age of 173.5 ± 1.5 Ma (MSWD = 0.02). This age correlates with the regional Jurassic magmatism postdating the Cimmerian orogeny and agrees with published magmatic ages (e.g., Çimen et al., 2018, 2017; Okay & Nikishin, 2015, and reference therein). Along the same transect, one sample was dated with AFT and three with AHe. The AFT cooling age is 53.6 ± 5.1 Ma, with a mean track length of 12.61 ± 2.44 μm based on 21 measurements. The AHe data reproduce well with cooling ages of 45.8 ± 6.6, 25.4 ± 3.3, and 29.5 ± 3.8 Ma from the highest to lowest sample.

5.1.3. RTZ and SEL Profiles

About 50 km west of the HAN profile, samples from two closely spaced vertical profiles (RTZ and SEL, Figures 2 and 3) yielded concordant U-Pb ages of 322.2 ± 2.7 and 309.8 ± 1.0 Ma (MSWD of 1.3 and 0.35, respectively, both from over 20 grains) in agreement with published geochronological data (e.g., Okay & Nikishin, 2015, and reference therein). The RTZ samples exhibit a ZHe cooling age of 113.5 ± 3.3 Ma and AFT cooling ages of 30.2 ± 1.6 and 27.4 ± 1.7 Ma, with mean track lengths of 13.30 ± 2.15 μm (100 measurements) and 13.02 ± 2.10 μm (84 measurements), respectively. These ages are comparable to three AHe cooling ages ranging from 33.2 ± 4.4 to 24 ± 2.1 Ma. The SEL profile yielded a ZHe cooling age of 66 ± 1.6 Ma and two AFT cooling ages of 35.2 ± 1.8 (mean track length of 13.79 ± 1.47 μm, 100 measurements) and 28.5 ± 2.7 Ma (mean track length of 12.84 ± 2.63 μm, but with only eight measurements), which overlap with three AHe cooling ages of 32.8 ± 4.0, 31.4 ± 3.7, and 30.9 ± 4.2 Ma.

5.1.4. KUR Profile

With an elevation range of ~500 m, the westernmost profile of the Küre Complex (KUR samples, Figures 2 and 3) yielded a zircon U-Pb concordant age of 169.4 ± 0.6 Ma (MSWD = 0.023, 26 grains) in agreement with published magmatic ages (e.g., Okay & Nikishin, 2015, and reference therein). AFT and AHe cooling ages exhibit a crude age-elevation relationship (Figures 2 and 3), with sample KUR-01 yielding AFT and AHe cooling ages of 70.6 ± 4.4 and 54.3 ± 10.6 Ma, respectively; KUR-11, having an AFT age of 64.5 ± 7.5 Ma (mean track length of 13.70 ± 3.12 μm from only 14 measurements) and an AHe age of 24.2 ± 3.2 Ma; KUR-04, with an AFT central age of 56.5 ± 4.9 Ma (mean track length of 13.76 ± 1.12 μm over 47 measurements; note that this sample did not pass the chi-square test; however, the age makes sense with the rest of the vertical profile, therefore we treat it as a single population) and an AHe age of 17.4 ± 2.5 Ma; and KUR-08, with an AFT pooled age of 34.8 ± 1.9 Ma and an AHe age of 11.4 ± 1.9 Ma. Unfortunately, the lowermost sample had few grains of relatively good quality with very low U and Th content and therefore was discarded, although it yielded two aliquots with a mean age of ~11 Ma (see supporting information).

5.1.5. Devrekani Basin

One sample was collected from the Devrekani Basin (DVK-03) and yielded a concordant Middle Jurassic U-Pb age of 169.4 ± 0.61 Ma (MSWD = 0.44, 13 grains) in agreement with published magmatic ages (Çimen et al., 2018, 2017); AFT and AHe cooling ages are 106.7 ± 5.1 and 81.5 ± 8.1 Ma, respectively (Figures 2 and 3). The mean track length is 15.51 ± 0.83 μm but was obtained from only 13 measurements.

5.2. Single and Multisample Thermal History Modeling

5.2.1. KOZ Profile

Single-sample and multisample thermal histories from the easternmost vertical profile depict major Cretaceous and Paleogene cooling episodes (Figures 5a and 5b). The amount of cooling during the Cretaceous event is poorly constrained; however, the peak temperature from the base of the Çağlayan Formation exposed near our granitoid samples is estimated to be ~100 °C (Derman & İztan, 1997). Therefore, if we consider an additional 1- to 3-km-thick section of rocks between the Çağlayan Formation and the granitoid, our samples may have experienced burial heating up to 130–160 °C. After that episode, samples remained within the AFT Partial Annealing Zone (PAZ) but below the AHe Partial Retention Zone (PRZ) until ~40 Ma, as recorded by a short-track population in the track-length distribution (Figure 5a). Between ~40 and 30 Ma, a second pulse of 70 to 90 °C of rapid cooling occurred (Figures 5a and 5b). This pulse was followed by a period of very slow cooling until the present (Figures 5a and 5b).

5.2.2. HAN Profile

Time-temperature paths of sample HAN-03 do not provide accurate information on the Cretaceous thermal history, but they illustrate the Paleocene cooling that started at ~60 to 50 Ma (Figure 5c). The amount of cooling associated with this event is poorly constrained; however, considering peak temperatures for the Çağlayan Formation of ~100 °C (Ekinveren oil seep; Derman & İztan, 1997; Korkmaz et al., 2013) and assuming an additional 2- to 4-km-thick section of rocks below it, the Cenozoic peak temperatures of our granitoid

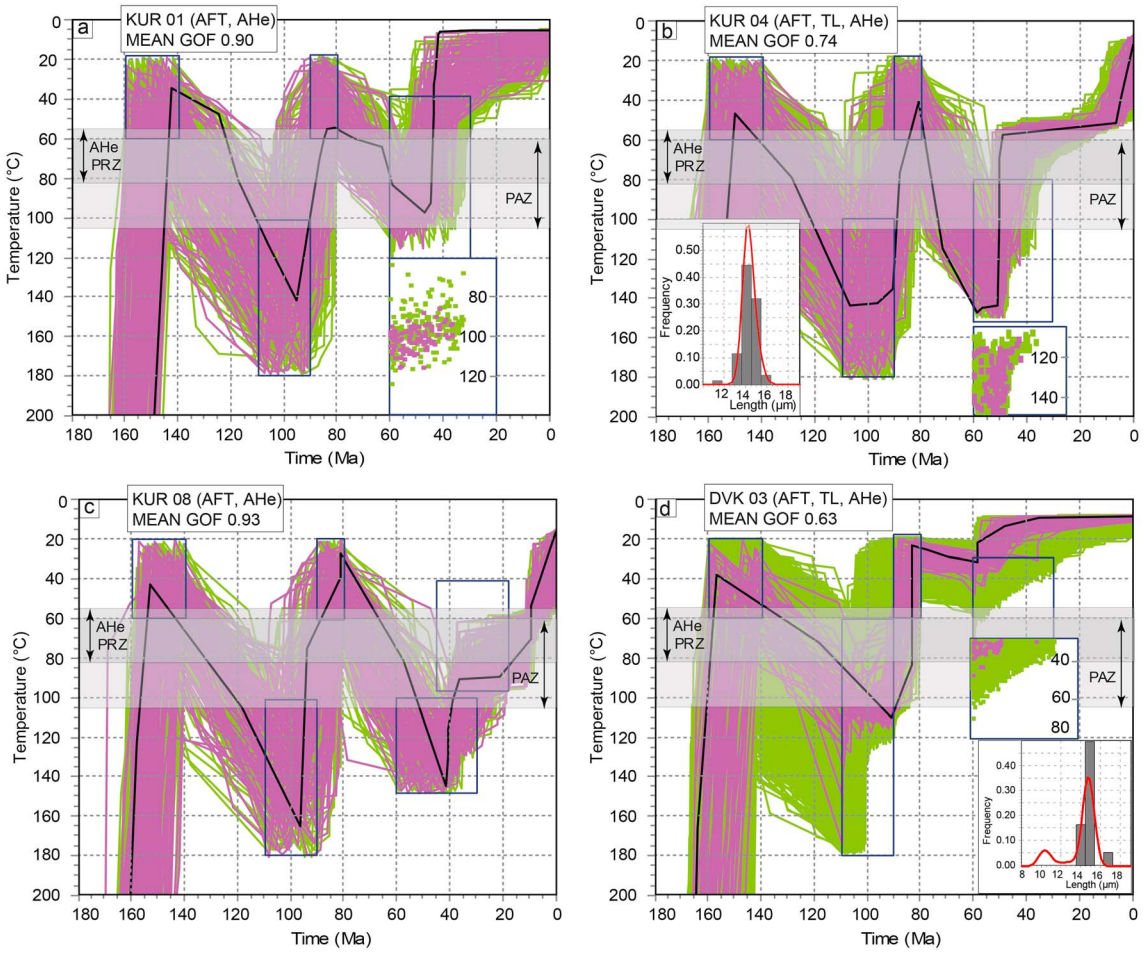

Figure 7. Inverse thermal modeling results for samples KUR (a–c) and the DVK (d; see caption of Figure 5 for details). The lack of track length data for sample KUR 08 (c) forced us to introduce an additional constraint box to simulate a path similar to those obtained for samples KUR 01 and 04.

should be 140–180 °C (see also constraint points in Figure 5c). Regarding the multisample modeling, it was not possible to obtain good or acceptable solutions, most likely because our AHe ages do not exhibit a typical age elevation relationship, but rather a scattered pattern (Figure 2c).

5.2.3. RTZ and SEL Profiles

Single-sample and multisample thermal modeling from the SEL elevation profile do not allow unraveling the Cretaceous thermal history. The occurrence of a ~66-My-old ZHe age, however, constrains the Paleocene peak temperatures to 190 to 210 °C (Figures 6a and 6b), in agreement with vitrinite reflectance and organic geochemistry data from the overlaying Çağlayan Formation (~165 °C; Derman & İztan, 1997; Görür & Tüysüz, 1997). For the RTZ vertical profile, the presence of a ~118 Ma ZHe cooling age limits Paleocene burial heating to temperatures <180 °C (Figures 6c and 6d). In both cases, this burial event was followed by 150 to 170 °C (SEL) and 110 to 140 °C (RTZ) cooling starting sometime between 60 and 40 Ma and accelerating from 40 to 25 Ma (Figures 6a and 6b).

5.2.4. KUR Profile

Samples from the KUR elevation profile exhibit high variability in AFT and AHe cooling ages with ~40-Myr difference over an elevation span of only 450 m (Table 1 and Figures 2 and 3). Unfortunately, the limited number of apatite crystals did not allow performing heavy-ion irradiations, and hence, thermal modeling was conducted using only AFT and AHe cooling ages, except for sample KUR-04, where about 50 track lengths were measured (Figure 7). While the software could not find acceptable paths in the multisample thermal modeling, single-sample thermal histories from the highest sample suggest 80–100 °C of rapid cooling across the PAZ and AHe PRZ between ~60 and 40 Ma followed by slow cooling from ~30 Ma to the present (KUR-01,

Figure 7a). Such an amount of cooling provides also constraints on the peak temperatures of the underlying samples that should be lower than 130 °C given the limited elevation range of the entire transect.

Paleogene cooling was also recorded by samples KUR-04 and KUR-08. Sample KUR-04 remained at the top of the AHe PRZ until ~15 Ma, when renewed rapid cooling started (~50 °C; Figure 7b). For sample KUR-08, the lack of track lengths prevented HeFTy from finding time-temperature paths similar to those obtained for sample KUR-01 and KUR-04, and hence, an additional constraint box at shallow depth was added between 40 and 30 Ma (Figures 7b and 7c). In any case, thermal histories from sample KUR-08 document at least ~60 °C of rapid cooling over the last ~11 Ma (Figure 7c), which is the most recent pulse of cooling recorded by our samples (Figure 8).

5.2.5. Devrekani Basin

Thermal histories of sample DVK-03 document burial heating of up to 110–120 °C in association with the deposition of Çağlayan Formation. This heating was followed by 60 to 100 °C of fast cooling between ~110 and 90 Ma, and subsequently by very slow cooling (10 to 50 °C) up to the present (Figure 7d). During the last 80 Myr, however, episodes of subsidence should have occurred, as documented by the occurrence of shallow to relatively deep marine, Upper Cretaceous to Eocene deposits in the Devrekani Basin (Figures 3 and 8). The occurrence of an ~80 Ma AHe cooling age suggests that any reheating would have not resulted in $T > 60$ °C to reset the AHe system, and hence, the post-80 Ma cooling history cannot be resolved by thermal modeling.

6. Discussion

Our new low-temperature thermochronology data and thermal modeling reveal at least three major pulses of rapid cooling (Figures 5–7). These events occurred during the Cretaceous (~110 to 90 Ma), the Paleogene (from ~60 to 40 Ma, followed by an acceleration from ~40 to 25 Ma), and the Late Miocene to Quaternary (<11 Ma) and were separated by phases of limited cooling or reheating (Figure 8). In the following sections, we will compare the spatiotemporal pattern of exhumation and burial with available stratigraphic data, and we will discuss the regional and local significance of our data in the framework of major Meso-Cenozoic geodynamic processes.

6.1. Late Cretaceous Cooling (~110 to 90 Ma): Exhumation of the Central Pontides Supercomplex Along the Central Pontides Active Margin

Time-temperature paths of the KOZ and DVK samples clearly document for the first time in the Central Pontides ~50 to 110 °C of Late Cretaceous cooling (Figures 5a, 5b, and 7d). This event appears to roughly coincide with regional tilting and erosion of the Barremian to earliest Albian (~130 to 110 Ma) Çağlayan Formation, which should have occurred sometime between 110 and 90 Ma (Albian to Coniacian; Figure 8). Such a tilting has been interpreted to represent the following: (1) long wavelength, thermally induced uplift (doming) along rift flanks preceding magmatic rifting (Hippolyte et al., 2010), (2) localized footwall uplift during the development of a horst and graben morphology associated with the opening of the Black Sea (Tüysüz et al., 2012), or (3) uplift during accretion and exhumation of the Central Pontides Supercomplex along the southern Eurasian margin (Aygül et al., 2016; Frassi et al., 2018; Okay et al., 2013). Although doming may have produced surface uplift and tilting, it seems unlikely that it may have also caused erosion of a 2- to 5-km-thick crustal section (see, e.g., the Central Kenya Dome, Spiegel et al., 2007). Furthermore, the cooling event recorded by our data predates rifting; it is not associated with syn-rift deposition, but rather with a sedimentary hiatus (Figure 8). Instead, our cooling ages could reflect exhumation of the HP-LT Central Pontides Supercomplex, possibly during trench roll back, slab steepening, and wedge extension (Aygül et al., 2016; Frassi et al., 2018; Okay et al., 2013). This interpretation is consistent with a coeval sedimentary hiatus, because tectonic denudation does not require significant erosional exhumation and accumulation of sediments in adjacent basins (e.g., Reiners & Brandon, 2006).

6.2. Late Cretaceous to Paleogene (~90 to 60 Ma) Synrift and Postrift Burial Heating

Our thermal histories show that the Late Cretaceous to Paleogene spatial pattern of burial heating was controlled by rifting processes associated with the opening of the Black Sea. For example, both the Devrekani Basin and the Sinop Range are in the hanging wall of the Ekinveren Fault (Figures 2 and 3); however, sample DVK underwent <60 °C of Cretaceous-Paleogene burial heating (Figure 7d), while most of samples from the Sinop Range experienced burial heating >120 °C (HAN samples, Figure 5c; SEL and RTZ samples, Figure 6;

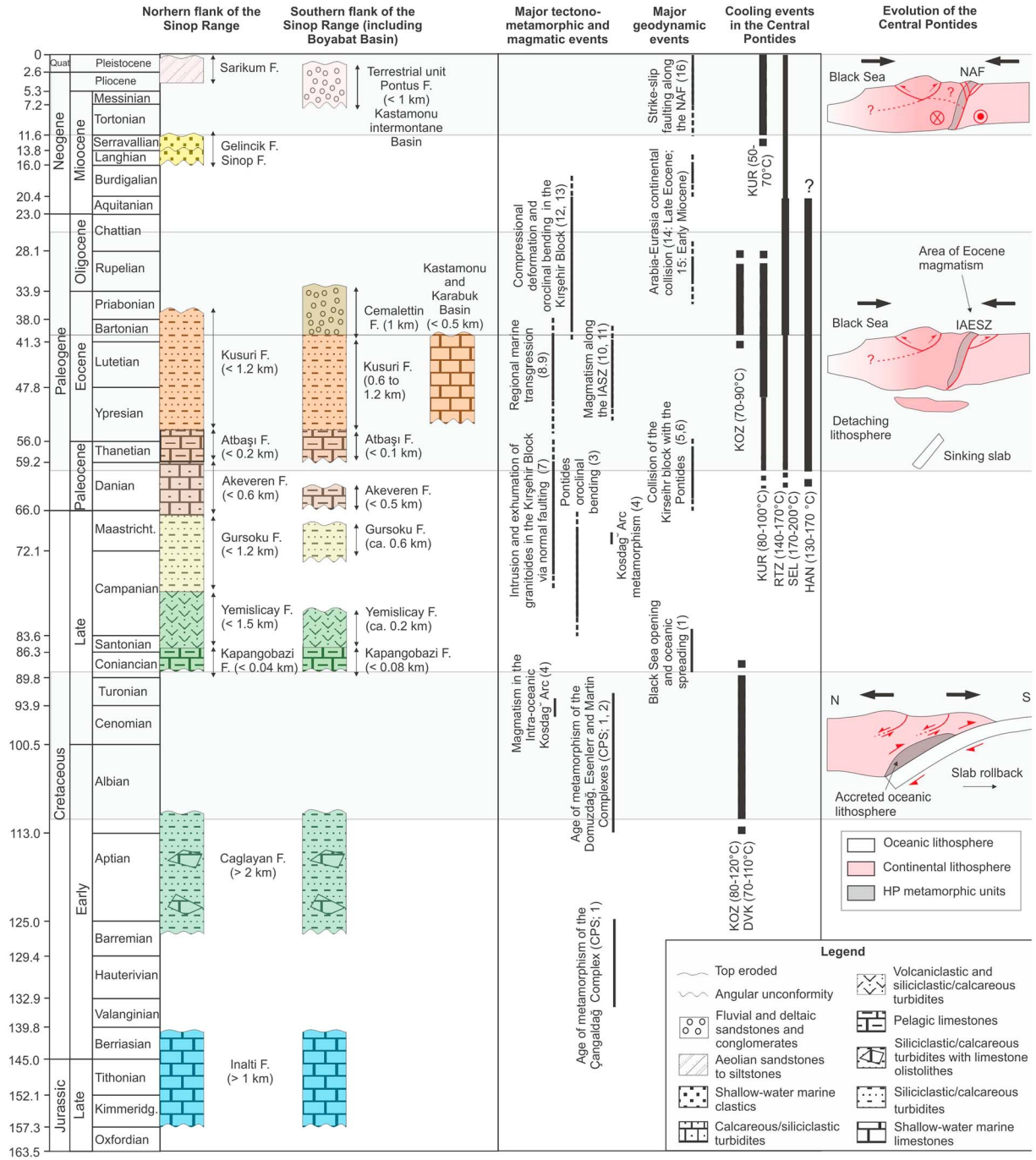

Figure 8. Simplified late Jurassic to Quaternary stratigraphy for the northern and southern slope of the Sinop range (with the thickness of each formation in parenthesis; Derman & İztan, 1997; Görür & Tüysüz, 1997; Hippolyte et al., 2010, 2015; Ilgar, 2014; Janbu et al., 2007; Leren et al., 2007; Okay et al., 2006, 2013, 2017; Tüysüz et al., 2012). Major regional and local tectonomagmatic, metamorphic, and geodynamic events are reported with a thin black line (from: 1, Okay et al., 2013; 2, Aygül et al., 2016; 3, Meijers et al., 2010; 4, Aygül & Oberhansli, 2015; 5, Okay et al., 2006; 6, Kaymakçı et al., 2009; 7 Van Hinsbergen et al., 2016; 8, Özcan et al., 2013; 9, Dinçer, 2016; 10, Topuz et al., 2005; 11, Göçmengil et al., 2018; 12, Lefebvre et al., 2013; 13, Gürer et al., 2016; 14, Boztuğ & Jonckheere, 2007; 15, Okay et al., 2010; 16, Şengör et al., 2005), while the timing and magnitude of cooling obtained in this study is shown with a thicker black line. Gray transparent polygons show major cooling events depicted by our modeling.

KUR samples, Figures 7b and 7c). This difference suggests the presence of a master normal fault between the Devrekani Basin and the Sinop Range, separating the interior of the Pontides from the southern margin of the Black Sea (Figures 2 and 3). Moreover, within the Sinop Range, there should have been a few horsts as documented by samples that experienced burial only up to peak temperatures of 100–120 °C (KOZ

samples, Figures 5a and 5b; KUR-01; Figure 7a). These differences in the Late Cretaceous and Paleogene burial history in the hanging wall of the Ekinveren Fault are consistent with stratigraphic data showing variable thicknesses (from more than ~4 km to less than ~2 km) of synrift to postrift Upper Cretaceous to Cenozoic sediments (Figure 8). Furthermore, a complex horst and graben configuration is still visible in seismic lines across the Black Sea shelf, where basin uplift and erosion has not occurred yet (e.g., the Sinop horst shown in Figure 3b; Espurt et al., 2014).

6.3. Paleocene Cooling (~60 to 40 Ma): Collision and Closure of the Northern Branch of the Neo-Tethys Ocean

Time-temperature paths of most of our samples document an onset of cooling from ~60 to 50 Ma (Figures 5–7). This event roughly correlates with tilting and erosion of the Gorsoku and Akeveren formations and older strata (Figure 8; Okay et al., 2006, 2013, 2017) and appears to roughly coincide with the syndepositional deformation recorded by Lower Eocene shallow-water marine limestones and clastic sediments deposited in the syncompressional piggyback Kastamonu and Karabük basins (Figures 2 and 8; Hippolyte et al., 2010). Our new cooling ages are also consistent with two AFT ages presented by Espurt et al. (2014; Figure 2) and Frassi et al. (2018; Figure 9), which have been used for documenting basin inversion of the Black Sea margin by 55 Ma. Furthermore, our ages are similar to sparse AFT cooling ages from the Western and the Central-Eastern Pontides (Figure 9; Boztuğ et al., 2004; Cavazza et al., 2011). Collectively, our data agree with previous studies suggesting that the final closure of the İzmir-Ankara-Erzincan branch of the northern Neo-Tethyan Ocean and the consequent collision between the southern Eurasian margin (Pontides) and the Kırşehir and Tauride-Anatolide microcontinental domains choked the subduction zone, leading to increased plate coupling, oroclinal bending, and widespread fault-related rock uplift and exhumation. (e.g., Boztuğ et al., 2004; Boztuğ & Jonckheere, 2007; Espurt et al., 2014; Hippolyte et al., 2010, 2015; Kaymakçı et al., 2009; Okay & Nikishin, 2015; Okay et al., 2006; Pourteau et al., 2016; Van Hinsbergen et al., 2016). It should be noted, however, that such a collision seems to postdate the Late Cretaceous (83 to 65 Ma) oroclinal bending in the Central Pontides (Meijers et al., 2010). A possible explanation could be that oroclinal bending processes took place during the collision between the intraoceanic Kosdağ magmatic arc (Aygül & Oberhansli, 2015) and the active Southern Eurasian margin. This scenario would imply that the Paleocene collision with the Kırşehir Block did not produce significant indentation and rotations along a vertical axis as previously thought (Kaymakçı et al., 2009; Meijers et al., 2010), but rather only fault-related exhumation.

6.4. Late Eocene to Late Oligocene Acceleration in Cooling (~40 to 25 Ma): Onset of the Arabia-Eurasia Continental Collision or Trench Advance?

Time-temperature paths of the KOZ, SEL, RTZ, and KUR samples document an acceleration in cooling rates from ~40 to 25 Ma. A similar pattern has been observed in the western Pontides (Figure 9; Cavazza et al., 2011; Okay et al., 2006), where it has been interpreted to reflect renewed tectonic activity along the İzmir-Ankara-Erzincan Suture zone during the final collision between the Kırşehir and Anatolide-Tauride microcontinental domains with the Pontides. As an alternative, the occurrence of Early Oligocene AFT cooling ages in the Kösedağ batholith to the east of the Kırşehir Block (Figure 9; Boztuğ & Jonckheere, 2007) and along the southern margin of the Anatolides and Taurides (e.g., Doğanşehir and Essence granitoids, Figure 9; Karaoğlan et al., 2016) has been interpreted to record the onset of continental collision between the Eurasian and Arabian plates (see also Rolland, 2017, and references therein). The occurrence of a regional compressional event that triggered an acceleration in fault-related exhumation from ~40 Ma, in association with syndepositional deformation, surface uplift, and oroclinal bending processes in the Kırşehir and Tauride-Anatolide microcontinental domains, is also documented by cross-cutting relationships, paleomagnetic, stratigraphic, and structural data (Figure 8; e.g., Advokaat et al., 2014; Aktaş & Robertson, 1984; Çetinkaplan et al., 2014; Clark & Robertson, 2002, 2005; Elmas & Yilmaz, 2003; Gürer et al., 2016, 2017; Jaffey & Robertson, 2005; Karaoğlan et al., 2013; Lefebvre et al., 2013; Nairn et al., 2013; Önal & Kaya, 2007; Pourteau et al., 2010; Robertson et al., 2006, 2007; Rolland, 2017). For example, stratigraphic data from the Kırşehir Block document compressional deformation from ~40 Ma after a phase of tectonic quiescence marked by a regional marine transgression associated with the deposition of nummulitic limestones (Figure 8; ~55–50 to 40–38 Ma; e.g., Advokaat et al., 2014; Clark & Robertson, 2002, 2005; Dinçer, 2016; Gürer et al., 2016, 2017; Jaffey & Robertson, 2005; Lefebvre et al., 2013; Licht et al., 2017; Özcan et al., 2013; Pourteau et al., 2010).

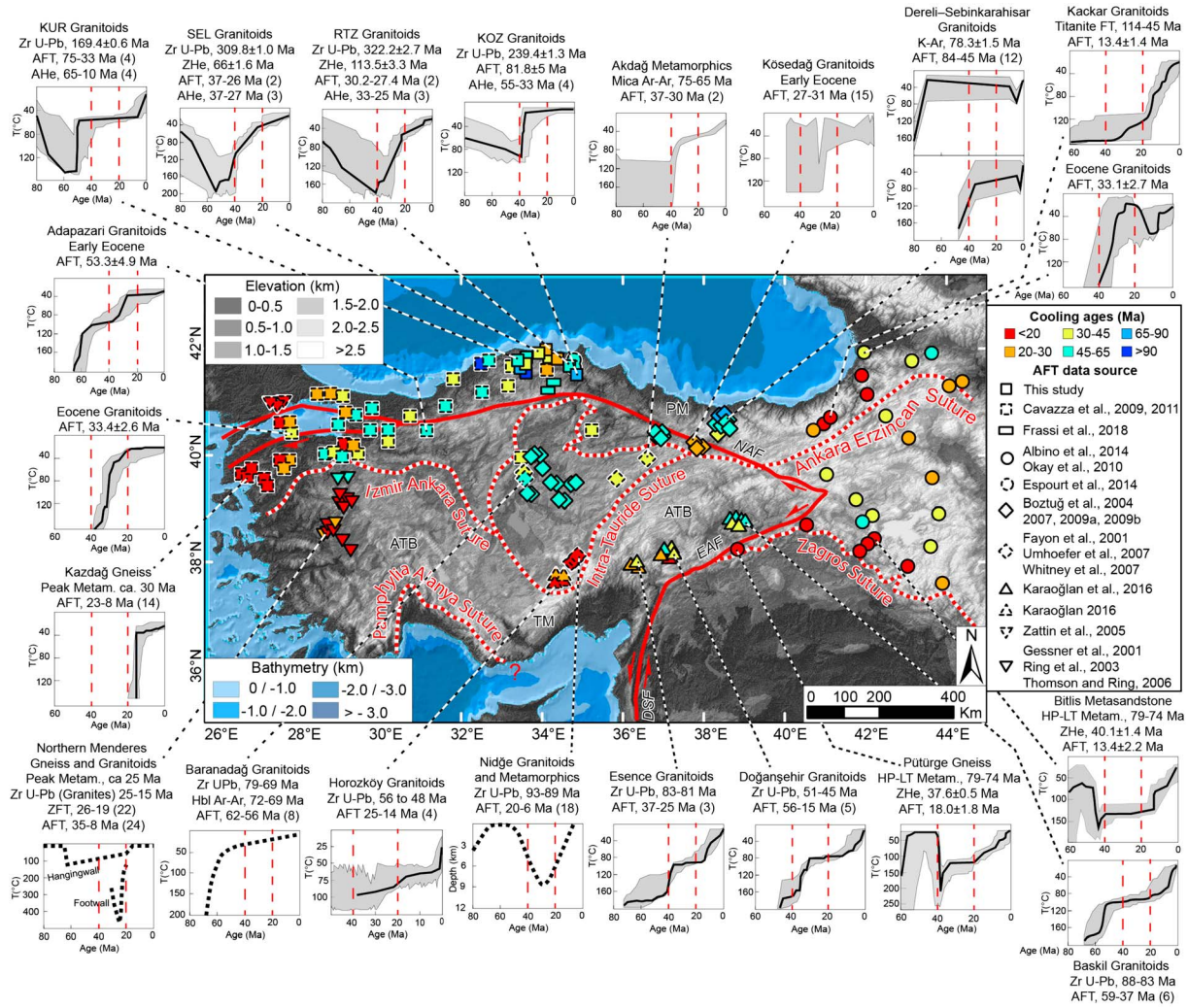

Figure 9. Digital Elevation Model of Turkey with available AFT cooling ages and representative time-temperature paths of granitoids and metamorphic samples with gray areas and black lines representing the envelope of good paths (GOF $>$ 0.5) and best fit models, respectively. Data and paths are from the sources cited in the legend except for the cooling history of the Baranadağ Granitoids, which is from Lefebvre et al. (2011). For each time-temperature path, a summary of available data, including zircon U-Pb (Zr U-Pb), mica Ar-Ar, zircon fission track (ZFT) and for our AHe sample ages is also provided. In the case of multiple ages, the age range is presented according to the error reported in the original publication with numbers in parenthesis representing the number of data points. Thermal modeling of samples from Okay et al. (2010), was obtained integrating AFT ages with unpublished AHe ages (Cavazza, personal communication).

To explore the regional spatial distribution of this erosional cooling event and its possible causes, we have compiled available AFT cooling ages and revised the most representative cooling histories from metamorphic and intrusive rocks throughout Anatolia (Figure 9). To differentiate magmatic from erosional cooling, we have included available ages from deeper thermochronometers or zircon U-Pb dating (Figure 9). Although S and SW Turkey are less represented, our compilation shows the occurrence of (1) a rapid cooling event at ~40 Ma across different terrains and (2) an additional acceleration of cooling at ~20 Ma mostly in eastern and western Turkey (but in W Turkey this cooling is related to extensional tectonics associated with the evolution of the Hellenic subduction zone; e.g., Faccenna et al., 2006). Given the widespread distribution of this latest Eocene cooling event, and considering that most terrains forming the Eurasian margin were already amalgamated by that time (e.g., Oberhänsli et al., 2012; Pourteau et al., 2016; Rolland, 2017; Van Hinsbergen et al., 2016), we favor the hypothesis that fault-related exhumation must have been triggered by major geodynamic changes along the southern Tethys subduction zone (which at that time extended from Makran to the Aegean Sea; e.g., Barrier & Vrielynck, 2008; Moix et al., 2008), rather than along the northern Tethys subduction zone which at that time was probably inactive (i.e., the İzmir-Ankara-Erzincan Suture Zone). This interpretation is consistent with the occurrence of Eocene volcanic rocks along the İzmir-

Table 2
Area Lost During Plate Convergence Over the Last 40 Ma

Region	Minimum values (km)	Maximum values (km)	References
Distance between N Arabia and S Taurides at 35 Ma (no margins included)	510	600	Van der Boon et al. (2018)
Distance between N Arabia and S Taurides from 40 to 35 Ma (no margins included)	150	160	McQuarrie and van Hinsbergen (2013)
Distance between Lesser and Greater Caucasus (Greater Caucasus Basin)	200	280	Van der Boon et al. (2018)
Total	860	1040	

Ankara-Erzincan Suture Zone, which have been interpreted to represent postcollisional magmatism triggered either by lithospheric delamination or slab break off (Figure 8; e.g., Göçmengil et al., 2018; Keskin et al., 2008; Topuz et al., 2005).

The regional exhumation event at ~40 Ma may be due to crustal shortening linked to (1) an increase in plate coupling during the subduction of the southern branch of the Neo-Tethys Ocean in association with trench advance (e.g., Heuret & Lallemand, 2005) or (2) the initial stages of the Arabia-Eurasia collision, when the stretched Arabian passive margin reached the subduction zone (*soft collision*) as proposed for Iran (Ballato et al., 2011). Possible reasons responsible for trench advance include lithosphere/upper mantle viscosity contrast between ~10^2 and 10^4 (Funicello et al., 2008), rapid motion of the upper plate away from the trench (Heuret & Lallemand, 2005), rapid motion of the subducting plate toward the trench (Schellart et al., 2008), subduction of wide slabs (trench parallel extent >4,000 km; Schellart et al., 2008), double subduction systems (Čížková & Bina, 2015), buckling of the subducting slab at the ~660 km mantle discontinuity (Čížková & Bina, 2015), and subduction of buoyant lithosphere (e.g., aseismic ridges, plateaus, and continental crust; Schellart et al., 2008, and references therein). In the case of the Late Eocene Neo-Tethys subduction system, some of these mechanisms appear to be unlikely (i.e., wide trench and double slab subduction), while others are difficult to prove given the lack of rheologic and kinematic constraints, and of indications on the paleo-oceanic floor and the paleodepth of the slab tip. With this respect, it should be noted that mantle tomography data suggest the occurrence of a positive seismic wave speed anomaly below the Bitlis Suture Zone up to 850 ± 100 km of depth, which may represent the Neo-Tethys slab (Van der Meer et al., 2018). This would suggest possible interactions between the slab tip and the 660 km mantle discontinuity, which may have induced changes in the kinematic regime of the overriding plate during the Cenozoic (Faccenna et al., 2013).

Regarding the second option, a recent plate-tectonic reconstruction suggests that the distance between northern Arabia and the southern Taurides-Anatolides at 35 Ma would have been 510 to 600 km (approximately 4.5 to 5.7° latitude, based on the position of continental edges that are currently in contact along the suture; Van der Boon et al., 2018), while at 40 Ma, such a distance would have been 660 to 760 km if we consider an additional 5 Myr of plate convergence at 30–32 mm/year (McQuarrie & van Hinsbergen, 2013). Furthermore, recent evidences suggest that suturing of Arabia with Eurasia was followed by the initiation of a new subduction zone south of the Greater Caucasus (Cowgill et al., 2016) in association with oroclinal bending in the Eastern Pontides-Lesser Caucasus and the closure of a supposed 200- to 280-km wide oceanic basin (Table 2; Van der Boon et al., 2018), which was in continuity with the Black and Caspian seas back-arc basins (Greater Caucasus Basin; Cowgill et al., 2016). Therefore, over the last 40 Myr, 860 to 1,040 km (Table 2) of plate convergence must have been accommodated in front of the Arabian indenter via different mechanisms (Table 3) such as (1) 80 to 230 km of upper plate shortening in the Bitlis, Taurides-Anatolides, Pontides,

Table 3
Mechanisms and Magnitude of Plate Convergence Accommodated in Front of the Arabian Indenter Over the Last 40 Ma

Deformation mechanisms	Minimum values (km)	Maximum values (km)	References
Greater Caucasus shortening	130	130	Cowgill et al. (2016)
Shortening in the Bitlis, Taurides-Anatolides, Pontides, and Lesser Caucasus	80	230	See text for details
Oroclinal bending and closure of the Greater Caucasus Basin	200	280	Van der Boon et al. (2018)
Arabian Plate shortening	50	80	Omar et al. (2015, and references therein)
Extrusion of Anatolia	50	70	See text for details
Total	510	790	

Note. The difference between the total plate convergence of Table 2 and the values below suggest 70 to 530 km of subduction of the Arabian passive margin.

and Lesser Caucasus, for a crustal thickening of 10 to 16 km, respectively (from 34 to 44 and 32 to 48 km, where both estimates include a ~2-km gain in elevation; Vanacore et al., 2013), and a current width (strike perpendicular) of the deformed collision zone in front of Arabia of 270 to 460 km, by assuming conservation of mass and in-plane pure shear deformation (with no erosion); (2) at least 130 km of upper plate shortening in the western Greater Caucasus (Cowgill et al., 2016); (3) 50 to 80 km of lower plate shortening as proposed for the Zagros Fold and Thrust Belt from NW Iran and Iraq (e.g., Omar et al., 2015, and references therein), which may be a lower limit, because if include shortening in the basement that so far has been documented only in Iran, we would have 150–180 km of lower plate shortening (Vergés et al., 2011); (4) 50 to 70 km from the extrusion of Anatolia, for a cumulative offset along the North Anatolian Fault of 85 ± 5 km (Şengör et al., 2005); and (5) 200 to 280 km of oroclinal bending in the Eastern Pontides-Lesser Caucasus and subduction below the Greater Caucasus (Van der Boon et al., 2018). These mechanisms would account for 510 to 790 km of plate convergence, while the remaining 70 to 530 km should have been accommodated through the subduction of the Arabian passive margin (Table 3). At the upper limit, 530 km of continental subduction should require a peculiar configuration, like an overthickened upper plate favoring eclogitization of the subducting plate, as recently suggested for the Indian margin (Ingalls et al., 2016), but this is not the case for Eastern Turkey. Conversely, 70 km of continental subduction is feasible, especially for a margin attached to a long oceanic slab (Ranalli et al., 2000; Regard et al., 2003; Royden, 1993), for a relatively rigid continental crust (i.e., with higher effective elastic thickness; Mouthereau et al., 2013) and for a high viscosity lower crust (i.e., with high coupling between lower crust and mantle lithosphere; Magni et al., 2012). The occurrence of a margin at least 70-km wide is also consistent with ophiolite obduction in Oman (~200 km over the Arabian margin; McQuarrie & van Hinsbergen, 2013) and with recent estimates on the length of the Arabian plate underthrust beneath Eurasia in Iran (150 km; Pirouz et al., 2017).

These estimations indicate that widespread exhumation at ~40 Ma could be related to the subduction of the stretched Arabian margin during the early stages of continental collision. Accordingly, accurate estimates of the magnitude of shortening and the width of the subducted Arabian continental margin prior to collision are crucial for decoding the collisional history of Arabia and Eurasia (Tables 2 and 3). In this context, the $<$20-Ma cooling event recorded between the Arabian Indenter and the Black Sea (Figure 9) and all around Iran (e.g., Ballato et al., 2013, 2015; Calzolari et al., 2015; Francois et al., 2014; Gavillot et al., 2010; Homke et al., 2010; Khadivi et al., 2012; Madanipour et al., 2017; Rezaeian et al., 2012) should represent a more advanced stage of collision, when subduction processes could not have accommodated any further plate convergence, and hence collision and indentation (*hard collision*, Ballato et al., 2011) became dominant.

Stratigraphic data from the suture zone (upper plate) and the Arabian foreland (lower plate) also indicate that shortening could have started by ~40 Ma. In the upper plate, an elongated (along strike), possibly continuous basin developed over the Bitlis-Pütürge continental Massif (Muş and Elazığ basins) and along the southern margin of the Taurides-Anatolides (Malatya Basin; Aksoy et al., 2005; Elmas & Yilmaz, 2003; Karaoğlan et al., 2013; Önal & Kaya, 2007; Robertson et al., 2006, 2007) during a short-lived phase of arc magmatism associated with extensional tectonics from ~52 to 45–40 Ma (Maden Group and Helete volcanics; Elmas & Yilmaz, 2003, and references therein). Sedimentation in these basins continued in a relatively deep marine system with the deposition of turbidites sourced from the N and NE throughout the Oligocene, and in a shallow marine system until the Early Miocene, when basin uplift and erosion occurred (Aksoy et al., 2005; Hüsing, et al., 2009; Rodelli et al., 2016). The presence of Oligocene deep-marine conditions has been interpreted to record either flexural subsidence during thrusting along the Bitlis-Zagros Suture Zone or extensional deformation associated with the late stages of Eocene extension (Hüsing, et al., 2009). Based on the lack of Oligocene volcanism and the regional cooling pattern highlighted in Figure 9, we favor the contractional option, which would agree with both hypotheses: trench advance and initial collision of the passive margin. Regarding the stratigraphy of the lower plate, the deposition of Middle Eocene shallow-marine limestones on the passive margin at the modern longitude of ~36°E was followed by a phase of regional uplift, tilting, and erosion until subsidence resumed with the deposition of unconformable Lower Miocene fluvial deposits (Boulton, 2009; Boulton & Robertson, 2007). Furthermore, the occurrence of ~16- to 11-M foreland-basin deposits in the footwall of the subduction thrust along the suture zone indicates that the contact between Eurasia and Arabia lithosphere must have occurred earlier than 16 Ma (Kahramanmaraş and Lice basins, Okay et al., 2010; Hüsing, et al., 2009, respectively). These observations would be consistent either with Late Eocene soft

collision followed by Early Miocene hard collision or trench advance with far-field transmission of regional stress during the Late Eocene followed by Early Miocene collision and plate suturing.

6.5. Late Miocene to Quaternary Cooling (<11 Ma): Extrusion of the Anatolian Microplate

Most of our thermal histories are characterized by a sharp decrease in Neogene cooling rates (Figures 5–7). This decline could be associated with a reduction of tectonic activity and the development of low-relief erosional surfaces, which are preserved in various locations along the Pontides (Figure 2). Samples from the KUR elevation profile, however, are an exception, as shown by the 11-Ma AHe cooling age (Table 1 and Figure 2) and thermal histories (Figure 6) that document ~50 °C of cooling since 11 Ma. This recent cooling event appears to roughly correlate with the progressive onset of the westward motion of Anatolia along the North Anatolian Fault, which is interpreted to have initiated in Eastern Anatolia at ~13 to 11 Ma (Şengör et al., 2005, and references therein). The strain localization that created this major structure is thought to have followed the termination of Arabia underthrusting beneath Eastern Anatolia (Hüsing et al., 2009) and slab break off of the southern Neo-Tethys Ocean (e.g., Capitanio, 2016; Faccenna et al., 2006; Keskin, 2003). Moreover, it may have also marked a decrease in oroclinal bending rates in the Eastern Pontides and Lesser Caucasus, where 50% of the curvature has been acquired between the Middle Eocene and the Late Miocene (Meijers et al., 2015). We suggest that our low-temperature thermochronology data document for the first time fault-related exhumation associated with activity along the broad restraining bend of the NAF. These data indicate that (1) deformation reached the Central Pontides shortly after the supposed onset of the westward motion of Anatolia (13–11 Ma; Şengör et al., 2005) and (2) initial deformation occurred over a large area around the NAF, as also documented in other sectors of the fault (i.e., the North Anatolian Shear Zone, Şengör et al., 2005, and references therein).

6.6. Paleogene (~60 to 25 Ma) Versus Neogene (<11 Ma) Exhumation Pattern

Our new cooling ages document a complex spatiotemporal pattern of fault-related exhumation associated with major Cenozoic shortening episodes. In particular, during the Paleogene, the highest magnitude of exhumation occurred in the central sectors of the Sinop Range and decreased to the east and west (Figure 10b). This cooling pattern suggests that exhumation was controlled by faulting along the Ekinveren Fault (Figure 10b). Moreover, the combination of these observations with our new data on exhumation and subsidence patterns during rifting and opening of the Black Sea (see sections 6.1 and 6.2) suggests that the north dipping Ekinveren Fault must represent an inverted normal fault, as also documented by published seismic lines along the easternmost sectors of the Sinop Range (Figure 3; Espurt et al., 2014). Consequently, the occurrence of Cretaceous AHe and AFT cooling ages in the basement of the Devrekani Basin (sample DVK) together with the occurrence of a thinner (<2 km), mostly postrift, sedimentary sequence capped by an extensive relict erosional surface, points to the existence of a major north-dipping blind fault (here called *Blind Ekinveren Fault*) north of the Devrekani Basin, where Cenozoic AHe and AFT cooling ages have been recorded (Figures 2 and 3).

Conversely, the Late Miocene to Quaternary spatial pattern of cooling suggests a westward increase in exhumation with virtually no exhumation in the eastern sectors of the Sinop Range (Figure 10b). This pattern is consistent with the preservation of the relict erosional surface near the KOZ vertical profile (Figure 2). There, thrusting along the Ekinveren Fault has produced only surface uplift with limited exhumation, while in the central western Sinop range, the lack of preserved remnant surfaces and the presence of high topographic relief coincide with the occurrence of our 11 Ma AHe cooling age (and associated greater exhumation). This spatial exhumation pattern is also compatible with increasing fault-normal strain rates along the western flank of the large restraining bend of the NAF (Yıldırım et al., 2011), where Global Positioning System data show the occurrence of a shortening component of up to 5 mm/year (Figures 10c and 10d). If we consider a modern surface temperature of ~10 °C, a geothermal gradient of ~25–30 °C, and a closure temperature for the AHe system of ~60 °C, we can estimate up to 2 km of exhumation for the western Sinop Range. This means that the relict low-relief erosional surface that has been eroded in the western Sinop Range could be placed 2 km above the lowermost sample of the KUR profile (Figures 10a and 10b). If we connect this inferred position of the relict surface with that one preserved in the eastern Sinop Range, we can extrapolate the pattern of maximum rock uplift for the entire Sinop Range, which mimics the exhumation pattern inferred from our cooling ages (Figure 10a). This reconstruction allows us to estimate not only the magnitude of rock uplift but also the amount of recent exhumation along the entire Sinop Range,

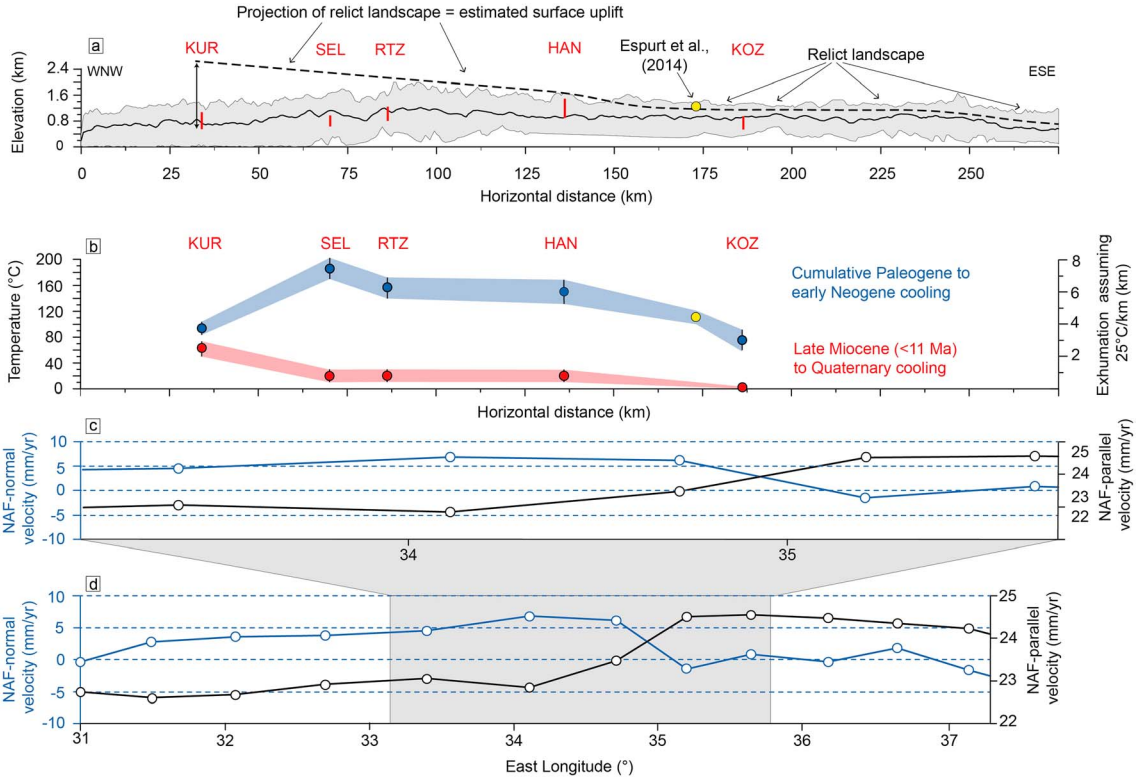

Figure 10. (a) Location of sampled vertical profiles (red thick line) projected over a topographic swath profile (see Figure 2 for location). The black dashed line represents the interpolation and the projection of the relict landscape (see Figure 2) for the eastern and western sectors, respectively (see text for further explanation). (b) Cumulative Paleogene and Late Cenozoic cooling and supposed exhumation. Note that the Paleogene pattern of cooling is characterized by a maximum in the central sectors of the Sinop Range, while in the Late Cenozoic, cooling was focused in the western sectors of the profile, where topographic relief is greater (see Figure 2). (c and d) Close-up (see black thick frame of Figure 10d for location) and regional view of Global Positioning System-derived fault normal (blue) and fault parallel (black) slip rates along the North Anatolian Fault (redrawn from Yıldırım et al., 2011), with positive fault-normal values indicating compression. Note that the Late Cenozoic cooling pattern roughly mimics the fault normal slip component of the North Anatolian Fault (NAF) and the inferred elevation of the relict landscape.

including areas that did not experience enough exhumation to yield Late Miocene or younger AHe cooling ages (Figure 10b). This exhumation pattern suggests that the Ekinveren Fault and its westernmost continuation (the Blind Ekinveren Fault) must have been reactivated as a pivotal fault pinned in its eastern sectors. Furthermore, it suggests that the superficial expression of the Ekinveren Fault south of the Devrekani Basin must represent a rather young fault, as also documented by deformed Quaternary deposits in its footwall (Yıldırım et al., 2011). In particular, it could represent a footwall short cut associated with Late Miocene to Quaternary faulting, and not a major fault responsible for the Cenozoic pattern of exhumation along the central western Sinop range.

7. Conclusions

Our low-temperature thermochronology and geochronology study from the Central Pontides offers the possibility to investigate the timing of fault-related exhumation associated with different geodynamic processes that occurred during the closure of the Neo-Tethys Ocean. In particular, we show that cooling (exhumation) occurred during multiple episodes that were separated by periods of limited cooling (slow erosion) and subsidence with sedimentation. The first cooling event occurred between ~110 and 90 Ma, most likely during exhumation of metamorphic rocks of the Central Pontides Supercomplex along a northward subducting branch of the northern Neo-Tethys Ocean. This event was followed by rifting and opening of the Black Sea and the development of a horst-and-graben morphology, which controlled the latest Cretaceous to earliest Cenozoic sedimentation and burial pattern along the Black Sea shelf. The Ekinveren Fault, which currently bounds the Sinop Range to the south, seems to represent one of the southernmost faults of this rift system. Renewed exhumation associated with basin inversion along the Ekinveren Fault took place during the

Paleocene from ~60 Ma, most likely during the collision of the Kırşehir and Tauride-Anatolide microcontinental domains with the Eurasian margin. This event was followed by accelerated cooling from ~40 to 25 Ma. From a regional compilation of low-temperature thermochronology data, we interpret the ~40-Ma event as a contractional deformation phase associated either with (1) the early stages of the Arabia-Eurasia continental collision, when the stretched passive margin reached the trench (soft collision) or (2) an increase in plate coupling triggered by trench advance, predating continental collision. Available shortening estimations can explain part of plate convergence history revealed by plate tectonic reconstructions, but a deficit of 70 to 530 km of convergence remains, which could be explained by the subduction of a stretched Arabian passive margin starting at ~40 Ma. The large uncertainty in the shortening-convergence budget shows that more accurate estimates are needed to clearly document the width of the subducted passive margin, and the main cause for this regional contractional event. In either case, our compilation shows that a second exhumation event occurred at ~20 Ma, most likely during the hard collision and the choking of the subduction zone. A final pulse of exhumation took place since ~11 Ma, possibly shortly after slab break-off beneath eastern Anatolia, and the onset of the westward motion of Anatolia at 13 to 11 Ma. This fault-related exhumation event appears to be controlled by the westward motion of Anatolia and the occurrence of a restraining band along the Northern Anatolian Fault. To date, contractional deformation along the Sinop Range associated with this deformation has produced widespread surface uplift, but $<$2 km of exhumation, and hence, it cannot be easily detected by low-temperature thermochronology. Collectively, our data highlight the importance of orogenic mobile belts as recorders of major geodynamic changes and associated deformation processes.

Acknowledgments

P. B., C. Y., and T.S. were funded by TOPO-EUROPE, an initiative of the European Science Foundation (project VAMP: Vertical Anatolian Movements Project) and by the EU Marie Skłodowska-Curie Actions program Initial Training Networks (ITN; project ALErT: Anatolian pLateau climatE and Tectonic hazards). T. S. and P. B. acknowledge support from the Emmy Noether Programm of the Deutsche Forschungsgemeinschaft (DFG) grant SCHI 1241/1-1 awarded to T. S. We are indebted to A. Çiner for logistical support and with C. Manntschke, P. Balling, and P. Catarraso for helping with sample preparation. We thank A. Okay, A. Pourteau, and R. Oberhänsli for introducing the geology of Turkey, C. Faccenna, F. Rossetti, D. Gürer, and G. Göçmengil for fruitful discussions and inspiration. Finally, we acknowledge Editor J. Geissman, Associate Editor O. Göğüş, one anonymous reviewer, L. Matenco, and D. van Hinsbergen for providing constructive revisions. Raw data can be found in the supporting information, while additional information is available from the authors upon request.

References

Advokaat, E. L., van Hinsbergen, D. J. J., Kaymakci, N., Vissers, R. L. M., & Hendriks, B. W. H. (2014). Late Cretaceous extension and Palaeogene rotation-related contraction in Central Anatolia recorded in the Ayhan-Büyükkışla basin. *International Geology Review*, *56*(15), 1813–1836. https://doi.org/10.1080/00206814.2014.954279

Aksoy, E., Türkmen, I., & Turan, M. (2005). Tectonics and sedimentation in convergent margin basins: An example from the Paleogene Elazığ Basin, eastern Turkey. *Journal of Asian Earth Sciences*, *25*, 459–472.

Aktaş, G., & Robertson, A. H. F. (1984). The Maden Complex, S.E.Turkey: Evolution of a Neotethyan continental margin. In J. E. Dixon, & A. H. F. Robertson (Eds.), *The geological evolution of the eastern Mediterranean*, *Special Publication*, (Vol. 17, pp. 375–402)). Oxford, UK: Geological Society of London.

Albino, I., Cavazza, W., Zattin, M., Okay, A. L., Adamia, S., & Sadradze, N. (2014). Far-field tectonic effects of the Arabia-Eurasia collision and the inception of the North Anatolian Fault system. *Geological Magazine*, *151*(2), 372–379. https://doi.org/10.1017/S0016756813000952

Alptekin, O., Nabelek, J. L., & Toksöz, M. N. (1986). Source mechanism of the Bartın earthquake of September 3, 1968, in northwestern Turkey: Evidence for active thrust faulting at the southern Black Sea margin. *Tectonophysics*, *122*(1-2), 73–88. https://doi.org/10.1016/0040-1951(86)90159-9

Aygül, M., & Oberhansli, R. (2015). Tectonic stacking of HP/LT metamorphic rocks in accretionary wedges and the role of shallowing slab-mantle decoupling. *Tectonics*, *36*, 1–15. https://doi.org/10.1002/2017TC004689

Aygül, M., Okay, A. I., Oberhansli, R., & Sudo, M. (2016). Pre–collisional accretionary growth of the Southern Laurasian active margin, Central Pontides, Turkey. *Tectonophysics*, *671*, 218–234. https://doi.org/10.1016/j.tecto.2016.01.010

Ballato, P., Landgraf, A., Schildgen, T. F., Stockli, D. F., Fox, M., Ghassemi, M. R., et al. (2015). The growth of a mountain belt forced by base-level fall: Tectonics and surface processes during the evolution of the Alborz Mountains, N Iran. *Earth and Planetary Science Letters*, *425*, 204–218. https://doi.org/10.1016/j.epsl.2015.05.051

Ballato, P., Stockli, D. F., Ghassemi, M. R., Landgraf, A., Strecker, M. R., Hassanzadeh, J., et al. (2013). Accommodation of transpressional strain in the Arabia-Eurasia collision zone: New constraints from (U-Th)/He thermochronology in the Alborz Mountains, N Iran. *Tectonics*, *32*, 1–18. https://doi.org/10.1029/2012TC003159

Ballato, P., Uba, C. E., Landgraf, A., Strecker, M. R., Sudo, M., Stockli, D. F., et al. (2011). Arabia-Eurasia continental collision: Insights from late Tertiary foreland-basin evolution in the Alborz mountains, northern Iran. *Geological Society of America Bulletin*, *123*(1-2), 106–131. https://doi.org/10.1130/B30091.1

Barrier, E., Vrielynck, B. (2008). Palaeotectonic map of the Middle East, Atlas of 14 maps, Tectonosedimentary-Palinspastic maps from Late Norian to Pliocene. Commission for the Geologic Map of the World (CCMW, CCGM), Paris, France.

Boulton, S. J. (2009). Record of Cenozoic sedimentation from the Amanos Mountains, southern Turkey: Implications for the inception and evolution of the Arabia-Eurasia continental collision. *Sedimentary Geology*, *216*(1-2), 29–47. https://doi.org/10.1016/j.sedgeo.2009.01.008

Boulton, S. J., & Robertson, A. H. F. (2007). The Miocene of the Hataya area, S Turkey: Transition from the Arabian passive margin to an underfilled foreland basin related closure of the southern Neotethys Ocean. *Sedimentary Geology*, *198*(1-2), 93–124. https://doi.org/10.1016/j.sedgeo.2006.12.001

Boztuğ, D., Güney, Ö., Heizler, M., Jonckheere, R. C., Tichomirowa, M., & Otlu, N. (2009a). $^{207}Pb^{206}Pb$, ^{40}Ar-^{39}Ar and fission-track geothermochronology quantifying cooling and exhumation history of the Kaman-Kırşehir region intrusions, central Anatolia, Turkey. *Turkish Journal of Earth Sciences*, *18*, 85–108.

Boztuğ, D., Jonckheere, R., Wagner, G. A., & Yeğingil, Z. (2004). Slow Senonian and fast Paleocene early Eocene uplift of the granitoids in the central eastern Pontides, Turkey: Apatite fission-track results. *Tectonophysics*, *382*(3-4), 213–228. https://doi.org/10.1016/j.tecto.2004.01.001

Boztuğ, D., & Jonckheere, R. C. (2007). Apatite fission track data from central Anatolian granitoids (Turkey): Constraints on Neo-Tethyan closure. *Tectonics*, *26*, TC3011. https://doi.org/10.1029/2006TC001988

Boztuğ, D., Türksever, E., Heizler, M., Jonckheere, R. C., & Tichomirowa, M. (2009b). $^{207}Pb^{206}Pb$, ^{40}Ar-^{39}Ar and apatite fission-track geothermochronology revealing the emplacement, cooling and exhumation history of the Karaçayir Syenite (N Sivas), East-Central Anatolian, Turkey. *Turkish Journal of Earth Sciences*, *18*, 109–125.

Braun, J., van der Beek, P., & Batt, G. (2006). *Quantitative thermochronology: Numerical methods for the interpretation of thermochronological data*. Cambridge, UK: Cambridge University Press. https://doi.org/10.1017/CBO9780511616433

Calzolari, G., Rossetti, F., Della Seta, M., Nozaem, R., Olivetti, V., Balestrieri, M. L., et al. (2015). Spatio-temporal evolution of intraplate strike-slip faulting: The Neogene-Quaternary Kuh-e-Faghan fault, Central Iran. *Geological Society of America Bulletin*, *128*(3-4), 374–396. https://doi.org/10.1130/B31266.1

Capitanio, F. A. (2016). The role of the Miocene-to-Pliocene transition in the Eastern Mediterranean extrusion tectonics: Constraints from numerical modeling. *Earth and Planetary Science Letters*, *448*, 122–132. https://doi.org/10.1016/j.epsl.2016.05.006

Cavazza, W., Federici, I., Okay, A. I., & Zattin, M. (2011). Apatite fission-track thermochronology of the Western Pontides (NW Turkey). *Geological Magazine*, *149*(1), 133–140.

Cavazza, W., Okay, A. I., & Zattin, M. (2009). Rapid early–middle Miocene exhumation of the Kazdag Massif (western Anatolia). *International Journal of Earth Sciences*, *98*(8), 1935–1947. https://doi.org/10.1007/s00531-008-0353-9

Çetinkaplan, M., Pourteau, A., Candan, O., Koralay, O. E., Oberhänsli, R., & Okay, A. L. (2014). P–T–t evolution of eclogite/blueschist facies metamorphism in Alanya Massif: Time and space relations with HP event in Bitlis Massif, Turkey. *International Journal of Earth Sciences*, *105*, 247–281.

Çimen, O., Göncüoğlu, M. C., Simonetti, A., & Sayit, K. (2017). Whole rock geochemistry, Zircon U-Pb and Hf isotope systematics of the Çangaldağ Pluton: Evidences for Middle Jurassic Continental Arc Magmatism in the Central Pontides, Turkey. *Lithos*, *290–291*, 136–155.

Çimen, O., Göncüoğlu, M. C., Simonetti, A., & Sayit, K. (2018). New zircon U-Pb LA-ICP-MS ages and Hf isotope data from the Central Pontides (Turkey): Geological and geodynamic constraints. *Journal of Geodynamics*, *116*, 23–36.

Čížková, H., & Bina, C. R. (2015). Geodynamics of trench advance: Insights froma Philippine-sea-style geometry. *Earth and Planetary Science Letters*, *430*, 408–415. https://doi.org/10.1016/j.epsl.2015.07.004

Clark, M., & Robertson, A. (2005). Uppermost Cretaceous–Lower Tertiary Ulukişla Basin, south-central Turkey: Sedimentary evolution of part of a unified basin complex within an evolving Neotethyan suture zone. *Sedimentary Geology*, *173*(1-4), 15–51. https://doi.org/10.1016/j.sedgeo.2003.12.010

Clark, M. S., & Robertson, A. H. F. (2002). The role of the Early Tertiary Ulukişla Basin, southern Turkey in suturing of the Mesozoic Tethys ocean. *Journal of the Geological Society, London*, *159*, 673–690.

Cowgill, E., Forte, A. M., Niemi, N., Avdeev, B., Tye, A., Trexler, C., et al. (2016). Relict basin closure accommodates continental convergence with minimal crustal shortening or deceleration of plate motion as inferred from detrital zircon provenance in the Caucasus. *Tectonics*, *35*, 2918–2947. https://doi.org/10.1002/2016TC004295

Derman, A. S., & İztan, Y. H. (1997). Results of geochemical analysis of seeps and potential source rocks from northern Turkey and the Turkish Black Sea. In A. G. Robinson (Ed.), *Regional and petroleum geology of the Black Sea and surrounding region*, (Vol. 68, pp. 313–330). Tulsa, OK: American Association of Petroleum Geologists Memoir.

Dinçer, F. (2016). Eocene benthic foraminiferal assemblages from Central Anatolia (Turkey): Biostratigraphy, stable isotope data, paleoenvironmental and paleontological interpretations. *Journal of Asian Earth Sciences*, *114*, 143–157.

Donelick, R. A., Ketcham, R. A., & Carlson, W. D. (1999). Variability of apatite fission-track annealing kinetics: II. Crystallographic orientation effects. *American Mineralogist*, *84*(9), 1224–1234. https://doi.org/10.2138/am-1999-0902

Dumitru, T. A. (1993). A new computer-automated microscope stage system for fission track analysis. *Nuclear Tracks and Radiation Measurement*, *21*(4), 575–580. https://doi.org/10.1016/1359-0189(93)90198-I

Ehlers, T. A., & Farley, K. A. (2003). Apatite (U-Th)/He thermochronometry: Methods and applications to problems in tectonic and surface processes. *Earth and Planetary Science Letters*, *206*(1-2), 1–14. https://doi.org/10.1016/S0012-821X(02)01069-5

Ellero, A., Ottria, G., Marroni, M., Pandolfi, L., & Goncuoglu, M. C. (2015). Analysis of the north anatolian shear zone in central Pontides (northern Turkey): Insight for geometries and kinematics of deformation structures in a transpressional zone. *Journal of Structural Geology*, *72*, 124–141. https://doi.org/10.1016/j.jsg.2014.12.003

Elmas, A., & Yilmaz, Y. (2003). Development of an oblique subduction zone: Tectonic evolution of the Tethys suture zone in southeast Turkey. *International Geology Review*, *45*(9), 827–840. https://doi.org/10.2747/0020-6814.45.9.827

Espurt, N., Hippolyte, J.-C., Kaymakci, N., & Sangu, E. (2014). Lithospheric structural control on inversion of the southern margin of the Black Sea Basin, Central Pontides, Turkey. *Lithosphere*, *6*(1), 26–34. https://doi.org/10.1130/L316.1

Faccenna, C., & Becker, T. W. (2010). Shaping mobile belts by small-scale convection. *Nature*, *465*(7298), 602–605. https://doi.org/10.1038/nature09064

Faccenna, C., Becker, T. W., Conrad, C. P., & Husson, L. (2013). Mountain building and mantle dynamics. *Tectonics*, *32*, 80–93. https://doi.org/10.1029/2012TC003176

Faccenna, C., Bellier, O., Martinod, J., Piromallo, C., & Regard, V. (2006). Slab detachment beneath eastern Anatolia: A possible cause for the formation of the North Anatolian fault. *Earth and Planetary Science Letters*, *242*(1-2), 85–97. https://doi.org/10.1016/j.epsl.2005.11.046

Farley, A., Wolf, R. A., & Silver, L. T. (1996). The effects of long alpha-stopping distances on (U-Th)/He ages. *Geochimica et Cosmochimica Acta*, *60*(21), 4223–4229. https://doi.org/10.1016/S0016-7037(96)00193-7

Farley, K. (2000). Helium diffusion from apatite; general behavior as illustrated by Durango fluorapatite. *Journal of Geophysical Research*, *105*(B2), 2903–2914. https://doi.org/10.1029/1999JB900348

Fayon, A. K., Whitney, D. L., Teyssier, C., Garver, J. I., & Dilek, Y. (2001). Effects of plate convergence obliquity on timing and mechanisms of exhumation of a mid-crustal terrain, the Central Anatolian Crystalline Complex. *Earth and Planetary Science Letters*, *192*(2), 191–205. https://doi.org/10.1016/S0012-821X(01)00440-X

Francois, T., Agard, P., Bernet, M., Meyer, B., Chung, S. L., Zarrinkoub, M. H., et al. (2014). Cenozoic exhumation of the internal Zagros: First constraints from low–temperature thermochronology and implications for the build–up of the Iranian plateau. *Lithos*, *206*, 100–112.

Frassi, C., Marroni, M., Pandolfi, L., Göncüoğlu, M. C., Ellero, A., Ottria, G., et al. (2018). Burial and exhumation history of the Daday Unit (Central Pontides, Turkey): Implications for the closure of the Intra-Pontide oceanic basin. *Geological Magazine*, *155*, 356–376.

Funicello, F., Facenna, C., Heuret, A., Lallemand, S., Di Giuseppe, E., & Becker, T. W. (2008). Trench migration, net rotation and slab–mantle coupling. *Earth and Planetary Science Letters*, *271*(1-4), 233–240. https://doi.org/10.1016/j.epsl.2008.04.006

Galbraith, R. F. (1981). On statistical models for fission-track counts. *Journal of Mathematical Geology*, *13*(6), 471–478. https://doi.org/10.1007/BF01034498

Gallagher, K. (2012). Transdimensional inverse thermal history modeling for quantitative thermochronology. *Journal of Geophysical Research*, *117*, B02408. https://doi.org/10.1029/2011JB008825

Gavillot, Y., Axen, G. J., Stockli, D. F., Horton, B. K., & Fakhari, M. D. (2010). Timing of thrust activity in the High Zagros fold-thrust belt, Iran, from (U-Th)/He thermochronometry. *Tectonics*, *29*, TC4025. https://doi.org/10.1029/2009TC002484

Gessner, K., Ring, U., Johnson, C., Hetzel, R., Passchier, C. W., & Güngör, T. (2001). An active bivergent rolling-hinge detachment system: Central Menderes metamorphic core complex in western Turkey. *Geology*, *29*(7), 611–614. https://doi.org/10.1130/0091-7613(2001)029%3C0611:AABRHD%3E2.0.CO;2

Gleadow, A. J. W., & Duddy, I. R. (1981). A natural long-term track annealing experiment for apatite. *Nuclear Tracks*, *5*(1-2), 169–174. https://doi.org/10.1016/0191-278X(81)90039-1

Gleadow, A. J. W., Gleadow, S. J., Belton, D. X., Kohn, B. P., Krochmal, M. S., & Brown, R. W. (2009). Coincidence mapping—A key strategy for the automatic counting of fission tracks in natural minerals. *Geological Society of London, Special Publication*, *324*(1), 25–36. https://doi.org/10.1144/SP324.2

Göçmengil, G., Karacık, Z., Genç, S. C., & Billor, Z. (2018). ^{40}Ar-^{39}Ar geochronology and petrogenesis of postcollisional trachytic volcanism along the İzmir-Ankara-Erzincan Suture Zone (NE, Turkey). *Turkish Journal of Earth Sciences*, *18*, 85–108.

Görür, N., & Tüysüz, O. (1997). Petroleum geology of the southern continental margin of the Black Sea. In A. G. Robinson (Ed.), *Regional and petroleum geology of the Black Sea and surrounding region*, *AAPG Memoir*, (Vol. 68, pp. 241–254).

Green, P. F. (1981). A new look at statistics in fission track dating. *Nuclear Tracks*, *5*(1-2), 77–86. https://doi.org/10.1016/0191-278X(81)90029-9

Gürer, D., van Hinsbergen, D. J. J., Matenco, L., Corfu, F., & Cascella, A. (2016). Kinematics of a former oceanic plate of the Neotethys revealed by deformation in the Ulukışla basin (Turkey). *Tectonics*, *35*, 2385–2416. https://doi.org/10.1002/2016TC004206

Gürer, D., van Hinsbergen, D. J. J., Ozkaptan, M., Creton, I., Koymans, M. R., Cascella, A., & Langereis, C. G. (2017). Paleomagnetic constraints on the timing and distribution of Cenozoic rotations in Central and Eastern Anatolia. *Solid Earth*. https://doi.org/10.5194/se-2017-66

Harrison, T. M., Watson, E. B., & Aikman, A. B. (2007). Temperature spectra of zircon crystallization in plutonic rocks. *Geology*, *35*, 635–638.

Heuret, A., & Lallemand, S. (2005). Plate motions, slab dynamics and back-arc deformation. *Physics of the Earth and Planetary Interiors*, *149*, 31–51.

Hippolyte, J. C., Espurt, N., Kaymakci, N., Sangu, E., & Müller, C. (2015). Cross-sectional anatomy and geodynamic evolution of the Central Pontide orogenic belt (northern Turkey). *International Journal of Earth Sciences*, 1–26.

Hippolyte, J.-C., Müller, C., Kaymakci, N., & Sangu, E. (2010). Dating of the Black Sea Basin: New nanoplankton ages from its inverted margin in the Central Pontides (Turkey). In R. A. Stephenson, et al. (Eds.), *Sedimentary basin tectonics from the Black Sea and Caucasus to the Arabian Platform*, *Special Publication*, (Vol. 340, pp. 113–136). Oxford, UK: Geological Society of London.

Homke, S., Vergés, J., Van Der Beek, P., Fernàndez, M., Saura, E., Barbero, L., et al. (2010). Insights in the exhumation history of the NW Zagros from bedrock and detrital apatite fission-track analysis: Evidence for a long-lived orogeny. *Basin Research*, *22*(5), 659–680. https://doi.org/10.1111/j.1365-2117.2009.00431.x

Hüsing, S. K., Zachariasse, W.-J., van Hinsbergen, D. J. J., Krijgsman, W., Inceoz, M., Harzhauser, M., et al. (2009). Oligocene Miocene basin evolution in SE Anatolia, Turkey: Constraints on the closure of the eastern Tethys gateway. In D. J. J. Van Hinsbergen, M. A. Edwards, & R. Govers (Eds.), *Collision and Collapse at the Africa–Arabia–Eurasia Subduction Zone*. *The Geological Society, London, Special Publications* (Vol. 311, pp. 107–132). Oxford, UK: Geological Society of London.

Hyndman, R. D., Currie, C. A., & Mazzotti, S. (2005). Subduction zone backarcs, mobile belts, and orogenic heat. *GSA Today*, *15*, 4–10.

Ilgar, A. (2014). Sedimentary record of mid-Miocene seismo-tectonic activity in the Sinop Peninsula, north-central Turkey. *Turkish Journal of Earth Sciences*, *23*, 16–30.

Ingalls, M., Rowley, D. B., Currie, B., & Colman, A. S. (2016). Large-scale subduction of continental crust implied by India–Asia mass-balance calculation. *Nature Geoscience*, *9*, 848–853.

Jaffey, N., & Robertson, A. (2005). Non-marine sedimentation associated with Oligocene-Recent exhumation and uplift of the Central Taurus Mountains, S Turkey. *Sedimentary Geology*, *173*(1–4), 53–89.

Janbu, N. E., Nemec, W., Kırman, E., & Ozaksoy, V. (2007). Facies anatomy of a channelized sand-rich turbiditic system: The Eocene Kusuri Formation in the Sinop Basin, north-central Turkey. In G. Nichols, C. Paola, & E. A. Williams (Eds.), *Sedimentary environments, processes and basins—A tribute to Peter Friend*, (Vol. 38, pp. 457–517). International Association of Sedimentologists.

Jonckheere, R., Enkelmann, E., Min, M., Trautmann, C., & Ratschbacher, L. (2007). Confined fission tracks in ion-irradiated and step-etched prismatic sections of Durango apatite. *Chemical Geology*, *242*(1–2), 202–217. https://doi.org/10.1016/j.chemgeo.2007.03.015

Karaoğlan, F. (2016). Tracking the uplift of the Bolkar Mountains (south-central Turkey): Evidence from apatite fission track thermochronology. *Turkish Journal of Earth Sciences*, *25*, 64–80.

Karaoğlan, F., Parlak, O., Hejl, E., Neubauer, F., & Klötzli, U. (2016). The temporal evolution of the active margin along the Southeast Anatolian Orogenic Belt (SE Turkey): Evidence from U–Pb, Ar–Ar and fission track chronology. *Gondwana Research*, *33*, 190–208. https://doi.org/10.1016/j.gr.2015.12.011

Karaoğlan, F., Parlak, O., Robertson, A., Thöni, M., Klötzli, U., Koller, F., & Okay, A. İ. (2013). Evidence of Eocene high-temperature/high-pressure metamorphism of ophiolitic rocks and granitoid intrusion related to Neotethyan subduction processes (Doğanşehir area, SE Anatolia). In A. H. F. Robertson, et al. (Eds.), *Geological development of Anatolia and the easternmost Mediterranean region*, *Special Publication*, (pp. 249–272). Oxford, UK: Geological Society of London.

Kaymakçı, N., Özçelik, Y., White, S. H., & van Dijk, P. M. (2009). Tectonostratigraphy of the Çankırı Basin: Late Cretaceous to early Miocene evolution of the Neotethyan Suture Zone in Turkey. In D. J. J. van Hinsbergen, et al. (Eds.), *Collision and collapse at the Africa–Arabia–Eurasia Subduction Zone*, *Special Publication*, (Vol. 311, pp. 67–106). Oxford, UK: Geological Society of London.

Keskin, M. (2003). Magma generation by slab steepening and breakoff beneath a subduction accretion complex: An alternative model for collision-related volcanism in Eastern Anatolia, Turkey. *Geophysical Research Letters*, *30*(24), 8046. https://doi.org/10.1029/2003GL018019

Keskin, M., Genç, Ş. C., & Tüysüz, O. (2008). Petrology and geochemistry of post-collisional Middle Eocene volcanic units in North-Central Turkey: Evidence for magma generation by slab breakoff following the closure of the Northern Neotethys Ocean. *Lithos*, *104*, 267–305.

Ketcham, R. A. (2005). Forward and inverse modeling of low-temperature thermochronometry data. In P. W. Reiners, & T. A. Ehlers (Eds.), *Low-temperature thermochronology*, (Vol. 58, pp. 275–314). Chantilly, VA: Reviews in Mineralogy and Geochemistry, Mineralogical Society of America.

Ketcham, R. A., Carter, A., Donelick, R. A., Barbarand, J., & Hurford, A. J. (2007). Improved modelling of fission-track annealing in apatite. *American Mineralogist*, *92*(5-6), 799–810. https://doi.org/10.2138/am.2007.2281

Ketcham, R. A., Donelick, R. A., Balestrieri, M. L., & Zattin, M. (2009). Reproducibility of apatite fissiontrack length data and thermal history reconstruction. *Earth and Planetary Science Letters*, *284*(3-4), 504–515. https://doi.org/10.1016/j.epsl.2009.05.015

Ketcham, R. A., Donelick, R. A., & Carlson, W. D. (1999). Variability of apatite fission-track annealing kinetics: III. Extrapolation to geological time scales. *American Mineralogist*, *84*(9), 1235–1255. https://doi.org/10.2138/am-1999-0903

Ketcham, R. A., Mora, A., & Parra, M. (2017). Deciphering exhumation and burial history with multi-sample down-well thermochronometric inverse modeling. *Basin Research*, *30*, 48–64. https://doi.org/10.1111/bre.12207

Khadivi, S., Mouthereau, F., Barbarand, J., Adatte, T., & Lacombe, O. (2012). Constraints on palaeodrainage evolution induced by uplift and exhumation on the southern flank of the Zagros-Iranian Plateau. *Journal of the Geological Society, London*, *169*(1), 83–97. https://doi.org/10.1144/0016-76492011-031

Korkmaz, S., Kara-Gulbay, R., & Istan, Y. H. (2013). Organic geochemistry of the Lower Cretaceous black shales and oil seep in the Sinop Basin, Northern Turkey: An oil-source rock correlation study. *Marine and Petroleum Geology*, *43*, 272–283. https://doi.org/10.1016/j.marpetgeo.2013.02.003

Lefebvre, C., Barnhoorn, A., van Hinsbergen, D. J. J., Kaymakci, N., & Vissers, R. L. M. (2011). Late Cretaceous extensional denudation along a marble detachment fault zone in the Kırşehir massif near Kaman, central Turkey. *Journal of Structrural Geology*, *33*, 1220–1236.

Lefebvre, C., Meijers, M. J. M., Kaymakci, N., Peynircioğlu, A., Langereis, C. G., & van Hinsbergen, D. J. J. (2013). Reconstructing the geometry of central Anatolia during the late Cretaceous: Large-scale Cenozoic rotations and deformation between the Pontides and Taurides. *Earth and Planetary Science Letters*, *366*, 83–98.

Leren, B. L. S., Janbu, N. E., Nemec, W., Kırman, E., & Ilgar, A. (2007). Late Cretaceous to Early Eocene sedimentation in the Sinop-Boyabat Basin, north-central Turkey: A deepwater turbiditic system evolving into littoral carbonate platform. In G. Nichols, C. Paola, & E. A. Williams (Eds.), *Sedimentary environments, processes and basins—A tribute to Peter Friend*, (Vol. 38, pp. 401–456). International Association of Sedimentologists.

Licht, A., Coster, P., Ocakoğlu, F., Campbell, C., Métais, G., Mulch, A., et al. (2017). Tectono-stratigraphy of the Orhaniye Basin, Turkey: Implications for collision chronology and Paleogene biogeography of central Anatolia. *Journal of Asian Earth Sciences*, *143*, 45–58. https://doi.org/10.1016/j.jseaes.2017.03.033

Ludwig, K. R. (2003). *Isoplot v. 3.0: A geochronological toolkit for microsoft excel*. Berkeley, CA: Berkeley Geochronology Center.

Madanipour, S., Ehlers, T. A., Yassaghi, A., & Enkelmann, E. (2017). Accelerated middle Miocene exhumation of the Talesh Mountains constrained by U-Th/He thermochronometry: Evidence for the Arabia-Eurasia collision in the NW Iranian Plateau. *Tectonics*, *36*, 1538–1561. https://doi.org/10.1002/2016TC004291

Magni, V., van Hunen, J., Funiciello, F., & Faccenna, C. (2012). Numerical models of slab migration in continental collision zones. *Solid Earth*, *3*(2), 293–306. https://doi.org/10.5194/se-3-293-2012

Mazzini, I., Hudačová, N., Joniak, P., Kováčová, M., Mikes, T., Mulch, A., et al. (2013). Paleoenvironmental and chronological constraints on the Tuğlu Formation (Çankırı Basin, Central Anatolia, Turkey). *Turkish Journal of Earth Sciences*, *22*, 747–777.

McKenzie, D. (1972). Active tectonics in the Mediterranean region. *Geophysical Journal of the Royal Astronomical Society*, *30*, 109–185.

McQuarrie, N., & van Hinsbergen, D. J. J. (2013). Retrodeforming the Arabia-Eurasia collision zone: Age of collision versus magnitude of continental subduction. *Geology*, *41*(3), 315–318.

Meijers, M. J., Smith, B., Pastor-Galán, D., Degenaar, R., Sadradze, N., Adamia, S., et al. (2015). Progressive orocline formation in the Eastern Pontides–Lesser Caucasus. In M. Sosson, et al. (Eds.), *Tectonic evolution of the eastern Black Sea and Caucasus*, *Special Publication* (Vol. 428, pp. 1–27). Oxford, UK: Geological Society of London.

Meijers, M. J. M., Kaymakci, N., Van Hinsbergen, D. J. J., Langereis, C. G., Stephenson, R. A., & Hippolyte, J.-C. (2010). Late Cretaceous to Paleocene oroclinal bending in the central Pontides (Turkey). *Tectonics*, *29*, TC4016. https://doi.org/10.1029/2009TC002620

Moix, P., Beccaletto, L., Kozur, H. W., Hochard, C., Rosselet, F., & Stampfl, G. M. (2008). A new classification of the Turkish terranes and sutures and its implication for the paleotectonic history of the region. *Tectonophysics*, *451*(1-4), 7–39. https://doi.org/10.1016/j.tecto.2007.11.044

Mouthereau, F., Watts, A. B., & Burov, E. (2013). Structure of orogenic belts controlled by lithosphere age. *Nature Geoscience*, *6*, 1–5.

Nairn, S. P., Robertson, A. H. F., Unlugenc, U. C., Tasli, K., & Inan, N. (2013). Tectonostratigraphic evolution of the Upper Cretaceous-Cenozoic central Anatolian basins: An integrated study of diachronous ocean basin closure and continental collision. *Geological Society of London, Special Publication*, *372*(1), 343–384. https://doi.org/10.1144/SP372.9

Nikishin, A. M., Korotaev, M. V., Ershov, A. V., & Brunet, M.-F. (2003). The Black Sea basin: Tectonic history and Neogene-Quaternary rapid subsidence modeling. *Sedimentary Geology*, *156*(1–4), 149–168. https://doi.org/10.1016/S0037-0738(02)00286-5

Nikishin, A. M., Okay, A., Tüysüz, O., Demirer, A., Wannier, M., Amelin, N., & Petrov, E. (2015). The Black Sea basins structure and history: New model based on new deep penetration regional seismic data. Part 2: Tectonic history and paleogeography. *Marine and Petroleum Geology*, *59*, 656–670. https://doi.org/10.1016/j.marpetgeo.2014.08.018

Nikishin, A. M., Okay, A. I., Tüysüz, O., Demirer, A., Amelin, N., & Petrov, E. (2015). The Black Sea basins structure and history: New model based on new deep penetration regional seismic data. Part 1: Basins structure and fill. *Marine and Petroleum Geology*, *59*, 638–655. https://doi.org/10.1016/j.marpetgeo.2014.08.017

Oberhänsli, R., Bousquet, R., Candan, O., & Okay, A. (2012). Dating subduction events in East Anatolia, Turkey. *Turkish Journal of Earth Sciences*, *21*, 1–17.

Okay, A. I., Altıner, D., & Kılıç, A. M. (2015). Triassic limestone, turbidite and serpentinite—Cimmeride orogeny in the Central Pontides. *Geological Magazine*, *152*(3), 460–479. https://doi.org/10.1017/S0016756814000429

Okay, A. I., Altiner, D., Sunal, G., Aygül, M., Akdoğan, R., Altiner, S., & Simmons, M. (2017). Geological evolution of the Central Pontides. In M. D. Simmons, G. C. Tari, & A. I. Okay (Eds.), *Petroleum Geology of the Black Sea*, *Special Publications*, (Vol. 464, 35 pp.). Oxford, UK: Geological Society of London.

Okay, A. I., & Nikishin, A. M. (2015). Tectonic evolution of the southern margin of Laurasia in the Black Sea region. *International Geology Review*, *57*(5–8), 1051–1076. https://doi.org/10.1080/00206814.2015.1010609

Okay, A. I., Şengör, A. M. C., & Görür, N. (1994). Kinematic history of the opening of the Black Sea and its effect on the surrounding regions. *Geology*, *22*(3), 267–270. https://doi.org/10.1130/0091-7613(1994)022%3C0267:KHOTOO%3E2.3.CO;2

Okay, A. I., Sunal, G., Sherlock, S., Altiner, D., Tüysüz, O., Kylander-Clark, A. R. C., & Aygül, M. (2013). Early Cretaceous sedimentation and orogeny on the southern active margin of Eurasia: Central Pontides, Turkey. *Tectonics*, *32*, 1247–1271. https://doi.org/10.1002/tect.20077

Okay, A. I., Sunal, G., Tüysüz, O., Sherlock, S., Keskin, M., & Kylander-Clark, A. R. C. (2014). Low-pressure–high temperature metamorphism during extension in a Jurassic magmatic arc, Central Pontides, Turkey. *Journal of Metamorphic Geology*, *32*(1), 49–69. https://doi.org/10.1111/jmg.12058

Okay, A. I., & Tüysüz, O. (1999). Tethyan sutures of northern Turkey. In B. Durand, et al. (Eds.), *The Mediterranean basins: Tertiary extension within the Alpine orogen*, *Special Publication*, (Vol. 156, pp. 75–515). Oxford, UK: Geological Society of London.

Okay, A. I., Tüysüz, O., Satir, M., Özkan-Altıner, S., Altiner, D., Sherlock, S., & Eren, R. H. (2006). Cretaceous and Triassic subduction-accretion, high-pressure-low-temperature metamorphism, and continental growth in the Central Pontides, Turkey. *Geological Society of America Bulletin*, *118*(9-10), 1247–1269. https://doi.org/10.1130/B25938.1

Okay, A. I., Zattin, M., & Cavazza, W. (2010). Apatite fission track data for the Miocene Arabia-Eurasia collision. *Geology*, *38*(1), 35–38. https://doi.org/10.1130/G30234.1

Omar, A. A., Lawa, F. A., & Sulalman, S. H. (2015). Tectonostratigraphic and structural imprints from balanced sections across the north-western Zagros fold-thrust belt, Kurdistan region, NE Iraq. *Arabian Journal of Geosciences*, *8*(10), 8107–8129. https://doi.org/10.1007/s12517-014-1682-6

Önal, M., & Kaya, M. (2007). Stratigraphy and tectono-sedimentary evolution of the Upper Cretaceous-Tertiary sequence in the southern part of the Malatya Basin, East Anatolia, Turkey. *Journal of Asian Earth Sciences*, *29*, 878–890.

Özcan, E., Less, G., & Kertesz, B. (2007). Late Ypresian to middle Lutetian Orthophragminid record from central and northern Turkey: Taxonomy and remarks on zonal scheme, Turk. *Journal of Earth Science*, *16*, 281–318.

Özcan, E., Özkan, R., Gül, M. A., Ercan, A., Alay, Z., Dinç, T., & Sinanlı, M. (2013). The Eocene shallow-marine transgressive events in central Anatolian Basins: The larger foraminiferal accumulations and foraminiferal compositions. pp. 311–316. 19th International Petroleum and Natural Gas Congress and Exhibition of Turkey, Ankara.

Özcan, Z., Okay, A. I., Özcan, E., Hakyemez, A., & Özkan-Altıner, S. (2012). Late Cretaceous–Eocene geological evolution of the Pontides based on new stratigraphic and palaeontologic data between the Black Sea coast and Bursa (NW Turkey). *Turkish Journal of Earth Sciences*, *21*, 933–960.

Özgen-Erdem, N., İnan, N., Akyazi, M., & Tunoğlu, C. (2005). Benthic foraminiferal assemblages and microfacies analysis of Paleocene-Eocene carbonate rocks in the Kastamonu region, Northern Turkey. *Journal of Asian Earth Sciences*, *25*, 403–417.

Özhan, G. (1989). A high resolution seismic reflection study in the Black Sea and geological consequences [in Turkish with English abstract]. *Geological Engineering*, *34–35*, 28e30.

Pirouz, M., Avouac, J.-P., Hassanzadeh, J., Kirschvink, J. L., & Bahroudi, A. (2017). Early Neogene foreland of the Zagros, implications for the initial closure of the Neo-Tethys and kinematics of crustal shortening. *Earth and Planetary Science Letters*, *477*, 168–182. https://doi.org/10.1016/j.epsl.2017.07.046

Pourteau, A., Candan, O., & Oberhänsli, R. (2010). High-pressure metasediments in central Turkey: Constraints on the Neotethyan closure history. *Tectonics*, *29*, TC5004. https://doi.org/10.1029/2009TC002650

Pourteau, A., Oberhänsli, R., Candan, O., Barrier, E., & Vrielynck, B. (2016). Neotethyan closure history of western Anatolia: A geodynamic discussion. *International Journal of Earth Sciences*, *105*(1), 203–224. https://doi.org/10.1007/s00531-015-1226-7

Ranalli, G., Pellegrini, R., & D'Offizi, S. (2000). Time dependence of negative buoyancy and the subduction of continental lithosphere. *Journal of Geodynamics*, *30*(5), 539–555. https://doi.org/10.1016/S0264-3707(00)00011-9

Rangin, C., Bader, A. G., Pascal, G., Ecevitoğlu, B., & Görür, N. (2002). Deep structure of the Mid-Black Sea High (onshore Turkey) imaged by multi-channel seismic survey (BLACKSIS cruise). *Marine Geology*, *182*, 265–278.

Regard, V., Faccenna, C., Martinod, J., Bellier, O., & Thomas, J. C. (2003). From subduction to collision: Control of deep processes on the evolution of convergent plate boundary. *Journal of Geophysical Research*, *108*(B4), 2208. https://doi.org/10.1029/2002JB001943

Reilinger, R., McClusky, S., Vernant, P., Lawrence, S., Ergintav, S., Cakmak, R., et al. (2006). GPS constraints on continental deformation in the Africa–Arabia–Eurasia continental collision zone and implications for the dynamics of plate interactions. *Journal of Geophysical Research*, *111*, B05411. https://doi.org/10.1029/2005JB004051

Reiners, P. W., & Brandon, M. T. (2006). Using thermochronology to understand orogenic erosion. *Annual Review of Earth and Planetary Sciences*, *34*, 419–466.

Rezaeian, M., Carter, A., Hovius, N., & Allen, M. B. (2012). Cenozoic exhumation history of the Alborz Mountains, Iran: New constraints from low temperature chronometry. *Tectonics*, *31*, TC2004. https://doi.org/10.1029/2011TC002974

Ring, U., Johnson, C., Hetzel, R., & Gessner, K. (2003). Tectonic denudation of a Late Cretaceous–Tertiary collisional belt: Regionally symmetric cooling patterns and their relation to extensional faults in the Anatolide belt of western Turkey. *Geological Magazine*, *140*(4), 421–441. https://doi.org/10.1017/S0016756803007878

Robertson, A. H. F., Parlak, O., Rizaoglu, T., Unlugenc, U., Inan, N., Tasli, K., & Ustaomer, T. (2007). Tectonic evolution of the South Tethyan ocean: Evidence from the Eastern Taurus Mountains (Elazig region, SE Turkey). In A. C. Ries, R. W. H. Butler, & R. H. Graham (Eds.), *Deformation of the Continental Crust: The Legacy of Mike Coward*, *Special Publication*, (pp. 231–270). Oxford, UK: Geological Society of London.

Robertson, A. H. F., Ustaömer, T., Parlak, O., Ünlügenç, U. C., Taşli, K., & İnan, N. (2006). The Berit transect of the Tauride thrust belt, S Turkey: Late Cretaceous–early Cenozoic accretionary/collisional processes related to closure of the southern Neotethys. *Journal of Asian Earth Sciences*, *27*(1), 108–145. https://doi.org/10.1016/j.jseaes.2005.02.004

Rodelli, D., Jovane, L., Özcan, E., Giorgioni, M., Coccioni, R., Frontalini, F., et al. (2016). High-resolution integrated magnetobiostratigraphy of a new middle Eocene section from the Neotethys (Elazığ Basin, eastern Turkey). *Geological Society of America*, *130*(1–2), 193–207.

Rolland, Y. (2017). Caucasus collisional history: Review of data from East Anatolia to West Iran. *Gondwana Research*, *49*, 130–146.

Royden, L. H. (1993). The tectonic expression slab pull at continental convergent boundaries. *Tectonics*, *12*(2), 303–325. https://doi.org/10.1029/92TC02248

Sato, K., Basei, M. A. S., Ferreira, C. M., Vlach, S. R. F., Ivanuch, W., Siga, Jr. O., & Onoi, A. T. (2010). In situ U-Th-Pb isotopic analyses by Excimer laser ablation/ICP–MS on Brazilian xenotime megacrystal: First U-Pb results at CPGeo-IG-USP. Paper presented at 7th South American Symposium on Isotope Geology. Brasília, Brasil.

Schellart, W. P., Stegman, D. R., & Freeman, J. (2008). Global trench migration velocities and slab migration induced upper mantle volume fluxes: Constraints to find an Earth reference frame based on minimizing viscous dissipation. *Earth Science Reviews*, *88*, 118–144.

Schemmel, F., Mikes, T., Rojay, B., & Mulch, A. (2013). The impact of topography on isotopes in precipitation across the Central Anatolian Plateau (Turkey). *American Journal of Science*, *313*(2), 61–80.

Schildgen, T. F., Yıldırım, C., Cosentino, D., & Strecker, M. R. (2014). Linking slab break-off, Hellenic trench retreat, and uplift of the Central and Eastern Anatolian plateaus. *Earth Science Reviews*, *128*, 147–168.

Şenel, M. (Ed.) (2002). Türkiye Jeoloji Haritası In *Geological Map of Turkey* (Sheets 19, scale 1:500,000). Maden Tetk. ve Arama, Genel Müdürlüğü, Ankara.

Şengör, Ä. M. C. (1991). Plate tectonics and orogenic research after 25 years: Synopsis of a Tethyan perspective. *Tectonophysics*, *187*, 315–334.

Şengör, A. M. C., Tüysüz, O., İmren, C., Sakınç, M., Eyidoğan, H., Görür, N., et al. (2005). The North Anatolian Fault: A new look. *Annual Review of Earth and Planetary Sciences*, *33*, 37–112.

Şengör, A. M. C., & Yılmaz, Y. (1981). Tethyan evolution of Turkey: A plate tectonic approach. *Tectonophysics*, *75*, 181–241.

Siqueira R., Hollanda, M. H. B. M. & Basei, M. A. S. (2014). A novel approach to (LA-ICP-MS acquired) U-Th-Pb data processing. Paper presented at 9th South American Symposium on Isotope Geology. São Paulo, Brasil.

Spiegel, C., Kohn, B. P., Belton, D. X., & Gleadow, A. J. W. (2007). Morphotectonic evolution of the central Kenya rift flanks: Implications for late Cenozoic environmental change in East Africa. *Geology*, *35*, 427–430.

Stampfli, G. M., & Borel, G. (2002). A plate tectonic model for the Paleozoic and Mesozoic constrained by dynamic plate boundaries and restored synthetic oceanic isochrons. *Earth and Planetary Science Letters*, *196*, 17–33.

Starostenko, V. I., Dolmaz, M. N., Kutas, R. I., Rusakov, O. M., Oksum, E., Hisarli, Z. M., et al. (2014). Thermal structure of the crust in the Black Sea: Comparative analysis of magnetic and heat flow data. *Marine Geophysical Researches*, *35*, 345–359.

Thomson, S. N., & Ring, U. (2006). Thermochronologic evaluation of postcollision extension in the Anatolide orogen, western Turkey. *Tectonics*, *25*, TC3005. https://doi.org/10.1029/2005TC001833

Topuz, G., Altherr, R., Schwarz, W. H., Siebel, W., Satır, M., & Dokuz, A. (2005). Post-collisional plutonism with adakite-like signatures: The Eocene Saraycık granodiorite (Eastern Pontides, Turkey). *Contributions to Mineralogy and Petrology*, *15*, 441–455.

Tüysüz, O., Yılmaz, İ. Ö., Švábenická, L., & Kirici, S. (2012). The Unaz Formation: A key unit in the western Black Sea Region, N Turkey. *Turkish Journal of Earth Sciences*, *21*, 1009–1028.

Umhoefer, P. J., Whitney, D. L., Teyssier, C., Fayon, A. K., Casale, G., & Heizler, M. T. (2007). Yoyo tectonic in a wrench zone, Central Anatolian fault zone, Turkey. In *Exhumation associated with continental strike-slip fault systems* (Vol. 434, pp. 35–57). Boulder, CO: Geological Society of America.

Ustaömer, T., & Robertson, A. H. F. (1994). Late Palaeozoic marginal basin and subduction-accretion: The Palaeotethyan Küre Complex, Central Pontides, northern Turkey. *Journal of the Geological Society, London*, *151*, 291–305.

Ustaömer, T., & Robertson, A. H. F. (1997). Tectonic-sedimentary evolution of the North-Tethyan margin in the Central Pontides of northern Turkey. In A. G. Robinson (Ed.), *Regional and petroleum geology of the Black Sea and surrounding region* (Vol. 68, pp. 255–290). Tulsa, OK: American Association of Petroleum Geologists Memoir.

Van der Boon, A., van Hinsbergen, D. J. J., Rezaeian, M., Gürer, D., Honarmand, M., Pasor Galan, D., et al. (2018). Quantifying Arabia–Eurasia convergence accommodated in the Greater Caucasus by paleomagnetic reconstruction. *Earth and Planetary Science Letters*, *482*, 454–469.

Van der Meer, D. G., van Hinsbergen, D. J. J., & Spakman, W. (2018). Atlas of the underworld: Slab remnants in the mantle, their sinking history, and a new outlook on lower mantle viscosity. *Tectonophysics*, *723*, 309–448.

Van Hinsbergen, D. J., Maffione, M., Plunder, A., Kaymakcı, N., Ganerød, M., Hendriks, B. W., et al. (2016). Tectonic evolution and paleogeography of the Kırşehir Block and the Central Anatolian Ophiolites, Turkey. *Tectonics*, *35*, 983–1014. https://doi.org/10.1002/2015TC004018

Vanacore, E., Taymaz, A. T., & Saygin, E. (2013). Moho structure of the Anatolian Plate from receiver function analysis. *Geophysical Journal International*, *193*, 329–337.

Vergés, J., Saura, E., Casciello, E., Fernàndez, M., Villaseñor, A., Jiménez-Munt, I., & Garcia-Castellanos, D. (2011). Crustal-scale cross-sections across the NW Zagros belt: Implications for the Arabian margin reconstruction. *Geological Magazine*, *148*(5–6), 739–761. https://doi.org/10.1017/S0016756811000331

Whitney, D. L., Teyssier, C., & Heizler, M. T. (2007). Gneiss domes, metamorphic core complexes, and wrench zones: Thermal and structural evolution of the Nigde Massif, central Anatolia. *Tectonics*, *26*, TC5002. https://doi.org/10.1029/2006TC002040

Willett, S. D., & Brandon, M. T. (2013). Some analytical methods for converting thermochronometric age to erosion rate. *Geochemistry, Geophysics, Geosystems*, *14*, 209–222. https://doi.org/10.1029/2012GC004279

Yıldırım, C., Melnick, D., Ballato, P., Schildgen, T. F., Echtler, H., Erginal, A. E., et al. (2013). Differential uplift along the northern margin of the Central Anatolian Plateau: Inferences from marine terraces. *Quaternary Science Reviews*, *81*, 12–28.

Yıldırım, C., Schildgen, T. F., Echtler, H., Melnick, D., Bookhagen, B., Çiner, A., et al. (2013). Tectonic and climatic implications of fluvial incision at the northern margin of the Central Anatolian Plateau based on multiple cosmogenic nuclides. *Tectonics*, *32*, 1–14. https://doi.org/10.1002/tect.20066

Yıldırım, C., Schildgen, T. F., Echtler, H., Melnick, D., & Strecker, M. R. (2011). Late Neogene orogenic uplift in the Central Pontides associated with the North Anatolian Fault—Implications for the northern margin of the Central Anatolian Plateau, Turkey. *Tectonics*, *30*, TC5005. https://doi.org/10.1029/2010TC002756

Yılmaz, Y. (2007). Morphotectonic evolution of the Southern Black Sea Region and the Bosphorus Channel. In V. Yanko-Hombach, et al. (Eds.), *The Black Sea flood question: Changes in the coastline, climate and human settlement*, (pp. 537–569). Dordrecht: Springer.

Zanchi, A., Zanchetta, S., Garzanti, E., Balini, M., Berra, F., Mattei, M., & Muttoni, G., (2009). The evolution of the Nakhlak-Anarak area, Central Iran, and its bearing for the reconstruction of the history of the Eurasian margin. In M. F. Brunet et al. (Eds.), *South Caspian to Central Iran Basins*. *The Geological Society, London, Special Publications* (Vol. 312, pp. 261–286). Oxford, UK: Geological Society of London.

Zattin, M., Okay, A. I., & Cavazza, W. (2005). Fission track evidence for late Oligocene and mid-Miocene activity along the North Anatolian Fault in southwestern Thrace. *Terra Nova*, *17*(2), 95–101.

Zonenshain, L. P., & Le Pichon, X. (1986). Deep basins of the Black-Sea and Caspian Sea as remnants of Mesozoic back-arc basins. *Tectonophysics*, *123*, 181–211.